MnDOT Contract, No. 1003325, Work Order No. 56

NRRA Long-term Research Project

Performance Benefits of Fiber-reinforced Thin Concrete Pavement and Overlays

TASKs 3 and 5 REPORT

Prepared by:

Manik Barman, Amarjeet Tiwari and Souvik Roy, UMD

and

Tom Burnham, Minnesota Department of Transportation

UMD
UNIVERSITY OF MINNESOTA DULUTH
Driven to Discover

DEPARTMENT OF TRANSPORTATION

2021

TABLE OF CONTENTS

LIST OF FIGURES

LIST OF TABLES

CHAPTER 1: INTRODUCTION

The Minnesota Department of Transportation (MnDOT) constructed two ultra-thin (thickness less than or equal to 4 inches) and six thin (thickness between 4-6 inches) concrete test cells at MnROAD in 2017. The MnROAD test facility is located on westbound I-94 near Otsego, northwest of the Twin Cities metropolitan area. These test cells were constructed as a part of a National Road Research Alliance (NRRA) funded long-term research study on fiber reinforced concrete. The main objective behind constructing these cells is to identify and quantify the contribution of structural fibers (macro-fibers) in mitigating different distresses that typically occur in thin and ultra-thin concrete pavements and overlays. Among the eight cells, seven were constructed with FRC, and one control cell was constructed with plain cement concrete. Two cells were constructed as unbonded concrete overlays on an existing concrete pavement, and the other six cells were ultra-thin and thin pavement cells constructed on an aggregate base layer. This report presents the works performed under the scopes of project Tasks 3 and 5. Task 3 deals with characterizing the influence of the structural fibers on fatigue cracking. Results of the ultrathin and thin pavements were used for this task and presented in Task 3. Task 5 deals with studying whether structural fibers can enable the use of larger slab sizes. Results of unbonded concrete overlay cells were used for this task and presented in Chapter 4.

CHAPTER 2: MNROAD TEST CELLS

2.1 Description of the Test Section

Table 1 presents the design details, and Figure 1 shows the location of test cells in the MnROAD test facility. Table 2 shows the construction time of different cells. Figure 2 to Figure 4 shows the section properties of all the seven FRC cells and one control cell, 506.

Cells 705 and 805 were constructed as overlays on an existing concrete pavement, which was constructed in 1993. All other cells were constructed as new pavement on a granular aggregate base. Cell 506 was constructed as the control cell with no fibers in it. Cells 139 and 239 were 3-inch and 4-inch thick, respectively, with enhanced fiber dosage, as noted in Table 1. Fiber dosages were decided either based on the residual strength ratio (RSR) or fiber volume fraction. The RSR, determined in accordance with ASTM 1609, is the ratio of flexural load at 120 mils (3 mm) mid-span deflection and the peak flexural load.

Cells 506, 706, and 806 were 5-inch thick pavement with varying fiber dosage as described in Table 1. Cell 606 was also planned to be constructed as 5-inch thick, but the thickness measured at multiple locations revealed that the as-built average thickness was closer to 6-inches.

A photograph of the fiber used in the construction is shown in Figure 5. The properties of this fiber can be found in Task 2B report for this project (MnDOT, 2018).

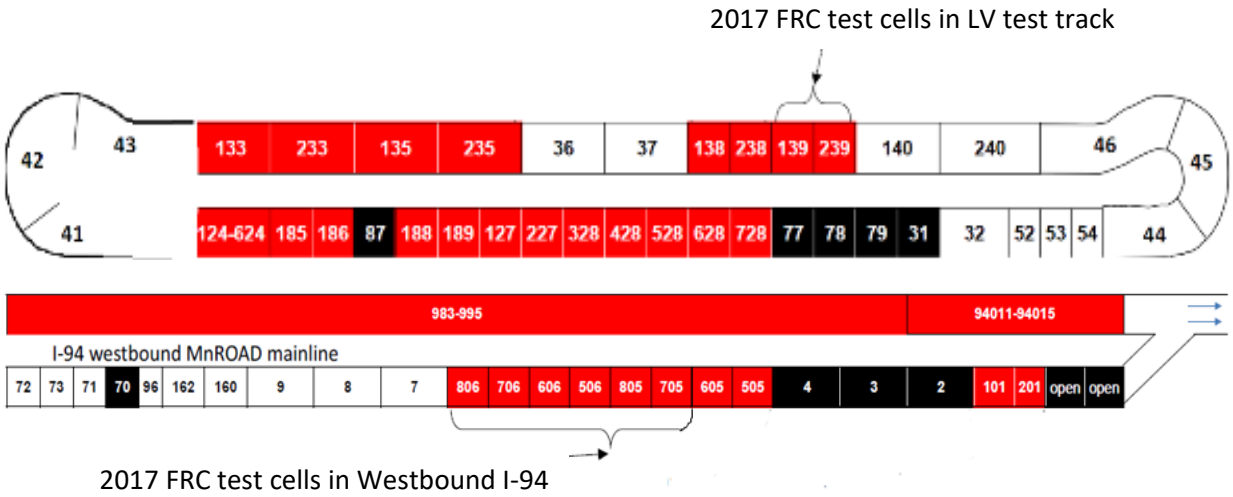

Figure 1: Location of the 2017 FRC research cells at the MnROAD test facility (MnDOT, 2018).

Table 1: Summary of the 2017 NRRA MnROAD test cells constructed for FRC study (MnDOT, 2018).

Cell number	Length (ft)	Pavement/ overlay Type	Underlying layer (constr. year)	Type of concrete/ fiber dosage*	Panel size W ft x L ft	Panel thickness (inch)
506	144	Thin pavement on gravel base	11 in. class 5Q aggregate base (2017)	*Plain concrete*	6 x 6	5
606**	138			*FRC/ standard*		
706				*FRC/ enhanced*		
806				*FRC/ high*		
139	270	Ultra-thin Pavement on gravel base	6 in. class 5 aggregate base (2017)	FRC/ enhanced	6 x 6	*3*
239	273	Thin Pavement on gravel base			6 x 6	*4*
705	144	Thin unbonded overlay on concrete pavement (w/fabric interlayer)	Concrete (1993)	FRC/ standard	*Driving: 14 x 12 Passing: 12 x 12*	5
805	124				*Driving: 6 x 12 and 8 x 12 Passing: 6 x 12 and 6 x 12*	5

** Fiber dosages: standard - corresponding to 20% residual strength ratio (ASTM C1609); enhanced - corresponding to 30% residual strength ratio (ASTM C1609); high – corresponding to 0.75 fibers volume fraction.*

*** Even though the design thickness was 5 inches, the actual measured thickness was found to be 6 inches*

Table 2: Paving date and time of the 2017 MnROAD FRC cells (MnDOT, 2018)

CELL	Date	Approximate Time
139	7/17/2017	9:15:00 AM
239	7/17/2017	9:15:00 AM
506	6/26/2017	9:20:00 AM
606	6/27/2017	9:15:00 AM
706	6/29/2017	8:45:00 AM
806	6/30/2017	8:00:00 AM
705	9/5/2017	2:00:00 PM
805	9/5/2017	3:00:00 PM

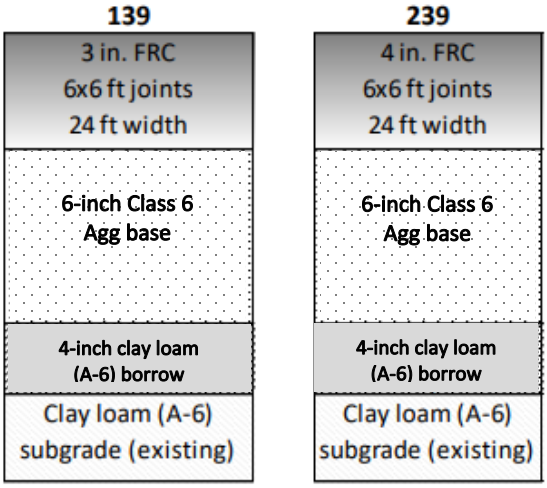

Figure 2: Section details for section 139 & 239 (MnDOT, 2018)

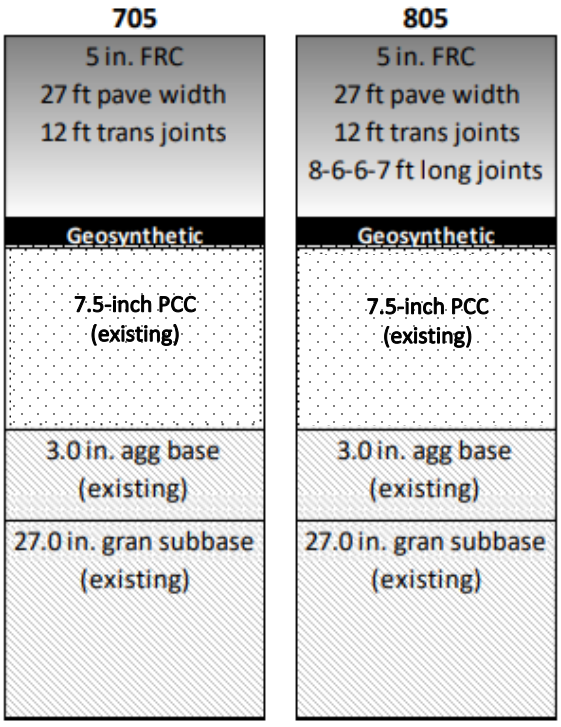

Figure 3: Section details for cells 705 and 805 (MnDOT, 2018)

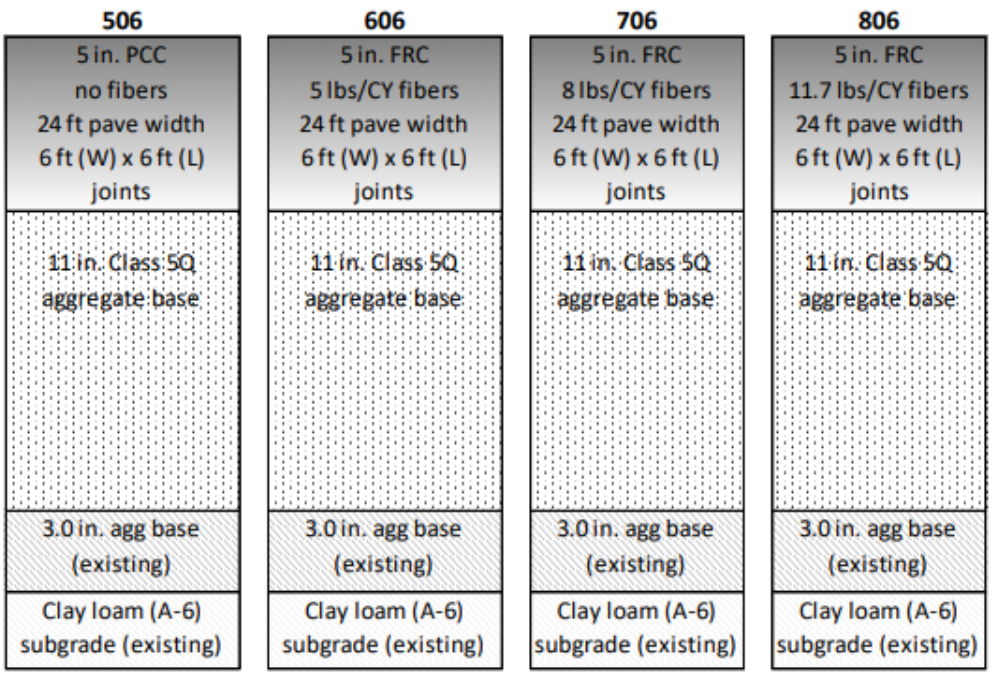

Figure 4: Section details for cells 506, 606, 706 and 806 (MnDOT, 2018)

Figure 5: Fibers used in the NRRA FRC study, 2017

2.2 Traffic Loading

MnROAD test facility has two different test segments, one with low volume traffic and the other with high-speed and high-volume traffic. Cells 139 and 239 were constructed on the low volume test track, which has two lanes, the inner and the outer lane. The inner lane is exposed to traffic loads provided by a 356-kN, 5-axle, tractor/trailer combination [3], which averages approximately 70 laps a day, equivalent to 30,000 to 40,000 concrete pavement ESALs per year depending on the thickness of the test cells. The outer lane is reserved for studying the influence of environmental loads only (no traffic)

Cells 506 to 806 and the two unbonded concrete overlay cells (Cells 705 and 805) were constructed on the high traffic volume test track adjacent to the original westbound I-94. During loading periods, two lanes of live interstate traffic is diverted to the test cells. These cells get approximately 1 million ESALs of loading per year.

2.3 Material Properties

2.3.1 Concrete mix design and other properties

Four different types of concrete mixes [6] were used for the present study. They are discussed as follows:

1. MR-3A21FC: This mix had zero fiber content and was used in the control Cell 506.

2. MR-3A21F1: This mix has a standard fiber dosage (i.e., with 20% RSR, 5 lb/cy fiber dosage). Cells 705, 805, and 606 contained this concrete mix.

3. MR-3A21F2: This mix has an enhanced fiber dosage (i.e., with 30% RSR, 8 lb/cy fiber dosage). This mix was used in Cells 139, 239, and 706.

4. MR-3A21F3: This mix had the highest amount of fiber dosage (0.75% fiber volume fraction, 11.7 lb/cy fiber dosage) and was used in Cell 806.

Table 3 shows the mix proportions for the above-mentioned four different types of concrete mixes. It shall be noted that the FRC mixes had a higher amount of cementitious material compared to the plain concrete mixes, and the cementitious material was increased with the fiber dosages. Additional paste content was needed for the increased surface area because of the fibers' inclusion in the mixture. The aggregate weights were adjusted to accommodate the additional cementitious materials.

Table 3: Mix design information for FRC cells (MnROAD, 2018).

Mix/Cell	Air (%)	Water (lbs)	Cement (lbs)	Fly ash (lbs)	Fly ash (%)	W/C Ratio	FA #1 (lbs)	CA #1 (lbs)	Fibers (lb/cy)	Fibers (% of conc. vol.)	Target RSR (%)	Slump range (in.)
MR-3A21FC/ 506	7.0	239	400	170	30	0.42	1222	1798	0	0	0	0.5-3
MR-3A21F1/ 705,805,606		248	413	177			1204	1773	5	0.33	20	
MR-3A21F2/ 139,239,706		252	420	180			1196	1761	8	0.52	30	
MR-3A21F3/ 806		258	430	185			1184	1743	11.7	0.75	NA	

Table 4 presents the test results of beams prepared at the project site for the ASTM C 1609 test. The average 28-day residual strength for the concrete used in Cells 606, 706, and 806 were 124, 156, and 254 psi, respectively. The average 28-day residual strength for Cells 139 and 239 was 185 psi, and it was 116.53 psi for Cells 705 and 805. The 28-day MORs for Cell 506, 606, 706, and 806 were 650, 635, 675, and 680 psi, respectively. The same for Cells 139 and 239 was 610 psi, and it was 542 psi for Cells 705 and 805. The other relevant fresh and hard concrete test results, including the ASTM C-1609 test results for all the cells, are provided in the APPENDIX.

Table 4: Measured properties of concretes used in the FRC research cells.

Cell number	Hardened concrete properties		
	28-day MOR (psi)	28-day residual strength (psi)	28-day RSR (%)
139	610	185	30.4
239			
705	542	116	21.5
805			
506	650	No applicable (NA)	NA
606	640	124	19.4
706	680	156	23.0
806	680	254	37.4

CHAPTER 3: TASK 3 FINDING ON FATIGUE CRACKING

3.1 Fatigue Crack Data

LTPP style cracking surveys were periodically conducted by MnDOT, with results recorded manually on MnROAD color-coded distress maps. Table 5 shows the different dates of the surveys, including the approximate ESALs accumulated by the date of each survey. Out of the eight test cells, Cell 139 was the thinnest test section, constructed with three-inch-thick (ultra-thin) fiber-reinforced concrete slabs on an unstabilized gravel base on the low-volume test track. Cell 139 was inadvertently exposed to early loads from construction trucks that were using the crossover segment to access other cells under construction, which resulted in many early-age cracks. These cracks continued to develop and propagated with age, and eventually, many slabs of this cell were shattered by the end of the summer of 2018, as shown in Figure 6. Besides that, there was a considerable amount of depression along the outer wheel path at some locations; this distress looked like rutting that occurs in asphalt pavements. Because of this cell's significantly different distress pattern compared to other cells (slab shattering vs fatigue cracking), Cell 139's crack data was not included in studying fibers' influence on the development of fatigue cracks.

Table 5: List of distress survey dates and accumulated ESALs.

Cell	Construction Dates in 2017	Distress Survey Dates in 2018/ ESALs	Distress Survey Dates in 2019 / ESALs	Distress survey Dates in 2020/ESALs
139	Jul 17	May 1/ 49K	Mar 18/ 82K; Dec 4/ 114K	Mar 24/ 195K
239	Jul 17	May 1/ 38K	Mar 18/ 62K; Dec 4/ 122K	Mar 24/ 146K
705	Sep 5	Mar 13/ 750K Apr 25/ 825K	Mar 18/ 1,800K; Oct 23/ 2,400K	Mar 5/2700K
805	Sep 5	Mar 13/ 750K; Apr 25/ 825K	Mar 18/ 1,800K; Oct 23/ 2,400K	Mar 5/2700K
506	Jun 26	Mar 14/ 750K	Mar 19/ 1,800K; Oct 25/ 2,400K	Mar 5/2700K
606	Jun 27	Mar 14/ 750K	Mar 19/ 1,800K; Oct 25/ 2,400K	Mar 5/2700K
706	Jun 29	Mar 14/ 750K	Mar 19/ 1,800K; Oct 25/ 2,400K	Mar 5/2700K
806	Jun 30	Mar 14/ 750K	Mar 19/ 1,800K; Oct 25/ 2,400K	Mar 5/2700K

Figure 6: Shattered slabs and depression along the wheel path in Cell 139.

Cell 239 on the low-volume test track is similar in all aspects to Cell 139, except it is a 4-inch thick. This cell experienced longitudinal and corner cracks, as shown in Figure 7. Some of the corner cracks along the shoulder were thought to be caused by the placement of the shouldering material. Figure 8 shows the consolidated distress map indicating the cracks measured at different seasons and years.

Figure 7: Corner and longitudinal cracks in Cell 239.

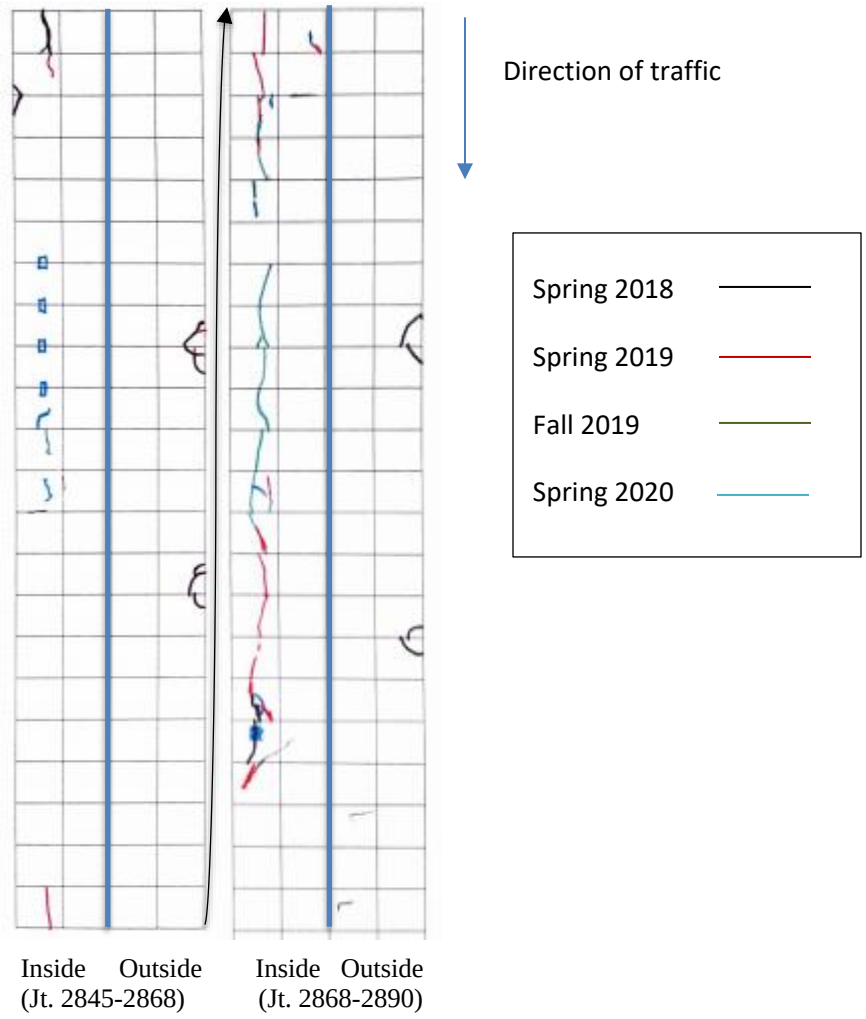

Figure 8: Color-coded distress map for Cell 239

Cells 506, 706, and 806 were constructed with 5-inch thick 6ft x 6ft size slabs on an unstabilized gravel base (not overlay). Cell 606 was unintentionally constructed with 6-inch thick 6ft x 6ft size slabs. All these cells were constructed on the mainline test track (I-94 westbound). Cell 506, which is the control cell constructed without any fibers, experienced transverse, and diagonal cracks in some slabs. Figure 9 shows a photograph of three distressed slabs of Cell 506 before they were replaced in June 2020. Figure 10 shows the color-coded distress map for Cells 506 and 606.

Figure 9: Cracks observed on Cell 506 (replaced in summer 2020).

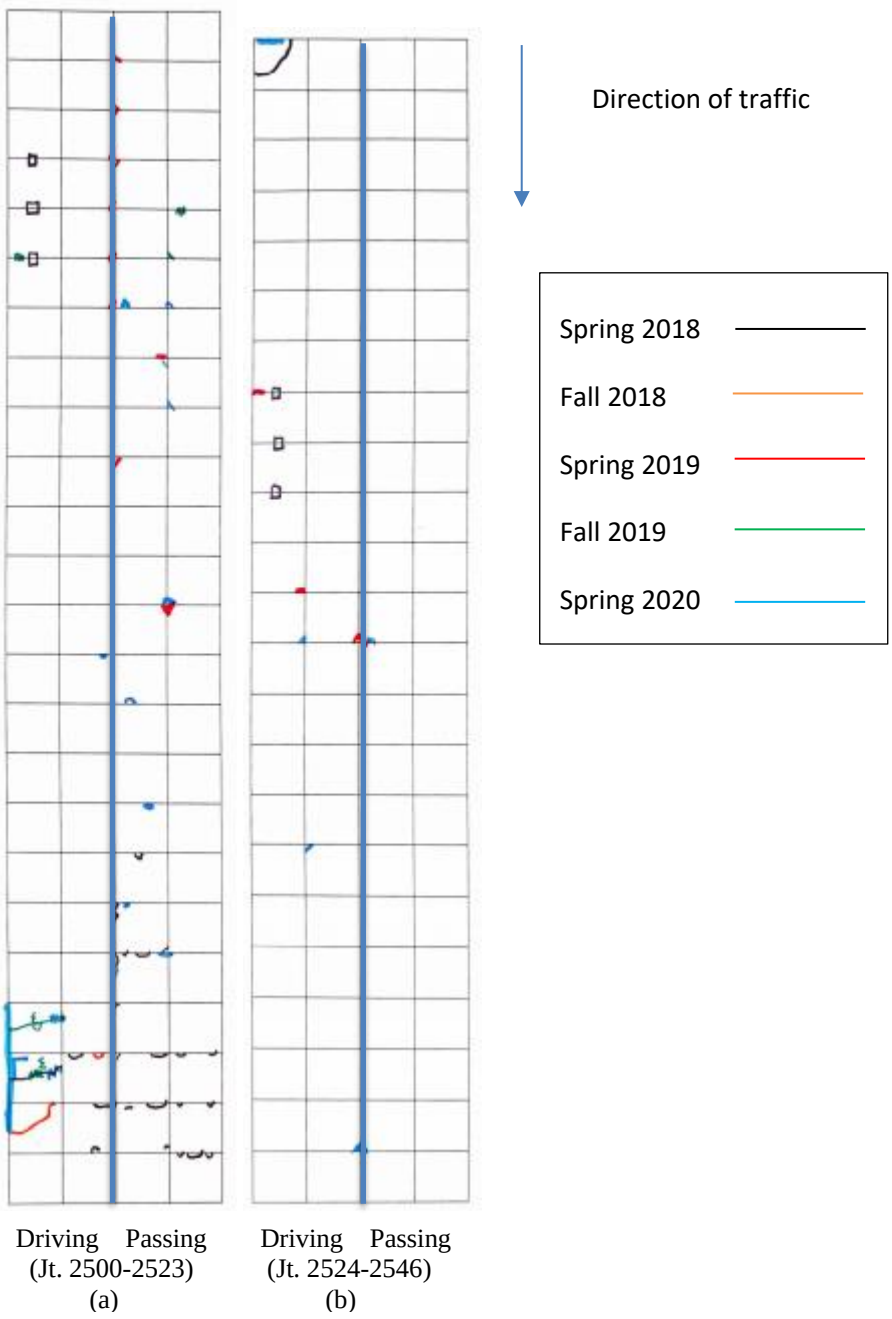

Figure 10: Distress Maps (a) Cell 506 (b) Cell 606.

Cell 606, which was constructed with 5 lbs./cy (20% residual strength) of structural fibers and 6 inches thick slabs, experienced one corner crack prior to April 2018; the severity of that crack did not change with age and ESALs. This crack is also located in the last panel next to a cell transition joint, so it can be assumed that this crack is not a typical fatigue-related crack; it occurred because of a construction issue.

The distress survey conducted on March 2020 found one joint spalling and two additional low severity corner cracks. Cells 706 and 806, which were constructed with fiber dosages of 8 and 11.7 lbs/cy, respectively, did not experience any cracks until March 2020 except for a couple of narrow cracks in Cell 806 that originated at the location of a joint opening sensor. A summary of the fatigue cracks documented in Cells 239 and 506 through 806 until March 2020 is provided in Figure 11. This figure does not include the unique distresses that developed in Cell 139. Comparison of Figure 8 and Figure 10 and Figure 11 show that 4-inch thick Cell 239 (with 8 lbs./cy fibers) has more visible cracks than 5-inch thick 506 and 6-inch thick 606 (with 5 lbs./cy fibers), despite significantly different traffic loadings.

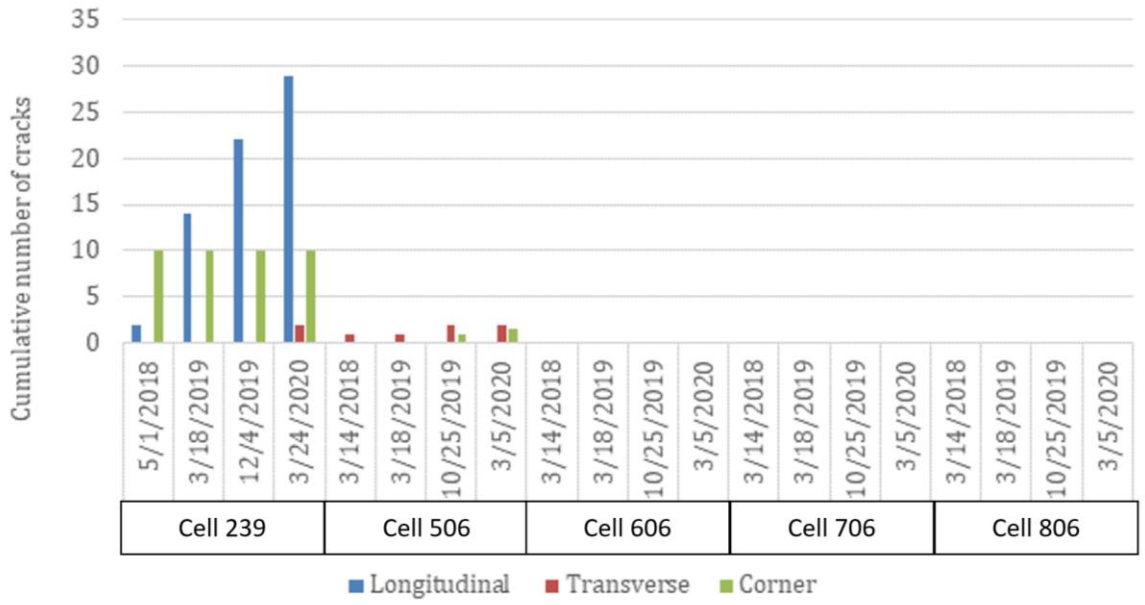

Figure 11: Summary of fatigue cracks of cells on gravel base until March 2020 (Cell 139 not shown).

3.2 Fatigue Crack Progression with Age and Traffic

Figure 12 shows the percentage of cracked slabs with respect to age (months) and ESALs for both lanes of Cells 239 and 506 through 806. Compared to the thin cells, ultrathin (4") Cell 239 resulted in significantly higher cracks. Approximately 20% of the slabs of Cell 239 had cracked by 150,000 ESALs; neither of the thin fiber-reinforced cells experienced that many cracked slabs even after 2.8 million ESALs. Figure 13 shows the percentage of cracked slabs only on the driving lanes. As much as 30% of the slabs in the driving lanes cracked after 2.8 million ESALs.

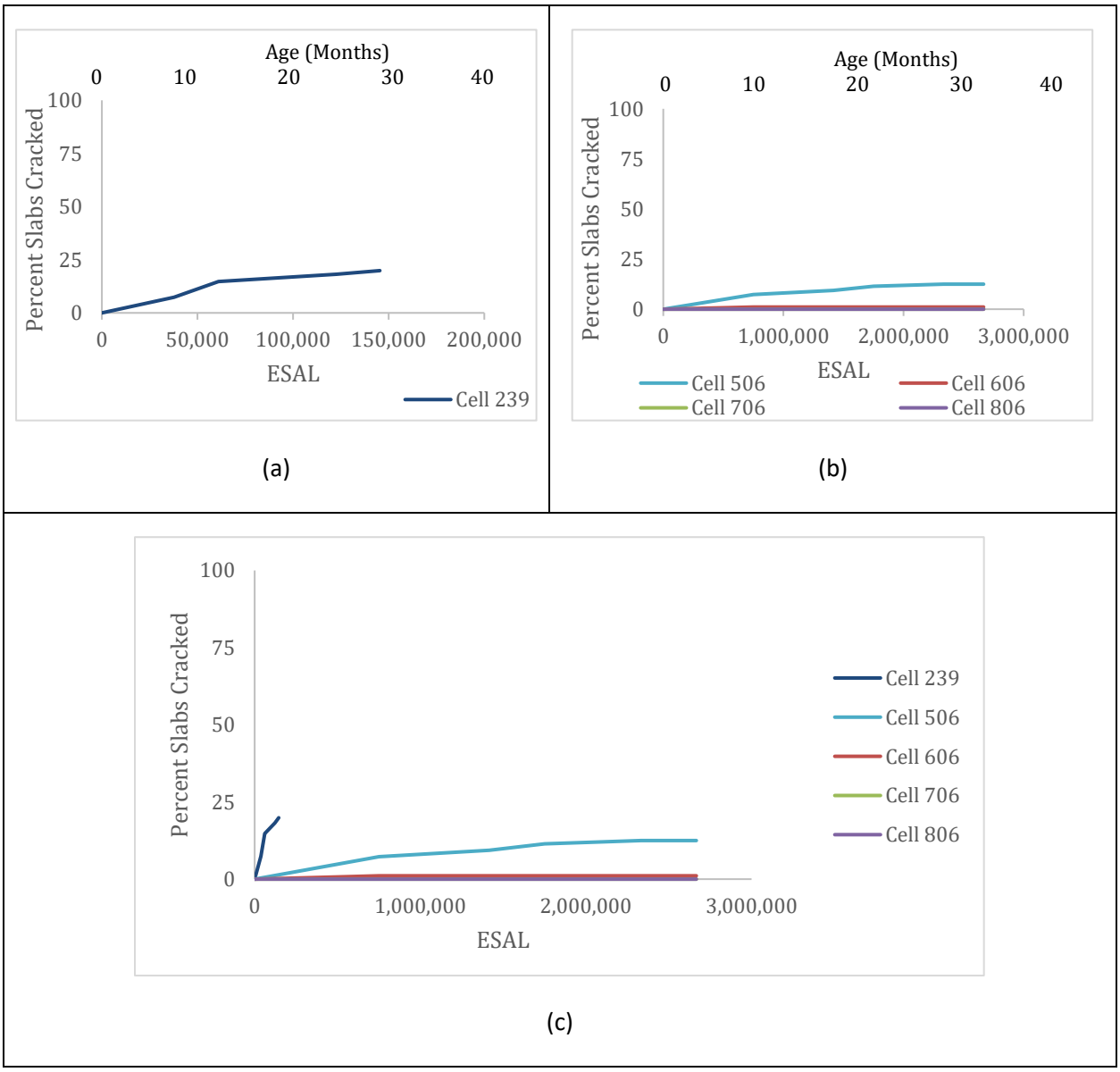

Figure 12: Percentage Crack vs. ESAL for both lanes (a) 239 (b) 506,606,706, and 806 (c) 239, 506, 606, 706, and 806

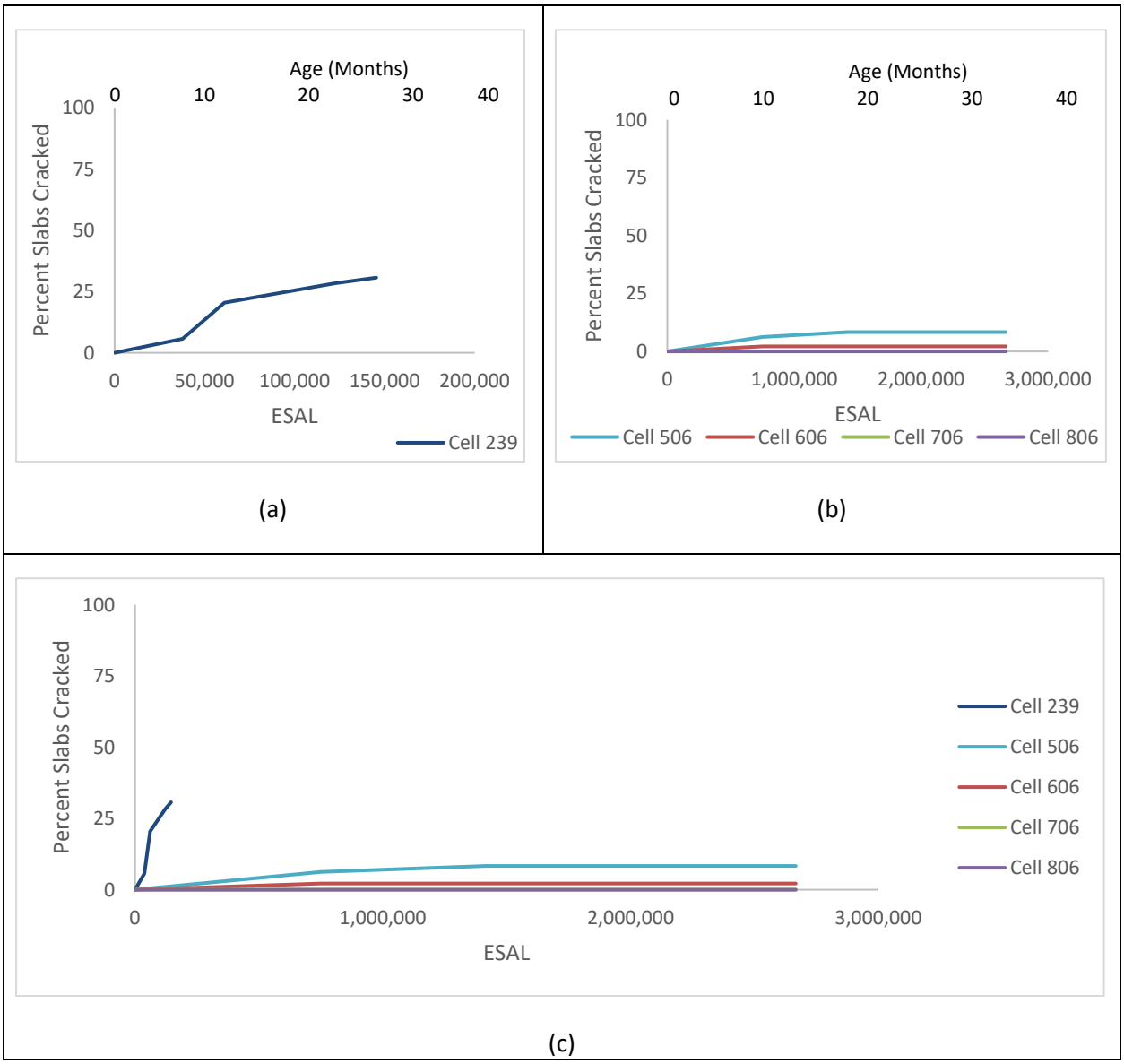

Figure 13: Percentage Crack vs. ESAL for the driving lane only (a) 239 (b) 506,606,706, and 806 (c) 239, 506, 606, 706, and 806.

While the number of cracks and the percentage of cracked slabs are good indicators to picture the overall cracking scenario, it does not distinguish between the small, medium, or long cracks. The crack length may be a better tool (than percent cracked slabs) to quantify the crack progression. The crack length vs ESAL relationship can even trace the crack propagation history. Figure 14 and Figure 15 compare the crack length between the cells for both lanes and for the driving lane (only), respectively. The total crack length for ultrathin Cell 239 was 184 feet compared to 44 feet for Cell 506 after three years of service. Only around 150,000 ESALs were enough to create a total of 184 feet in Cell 239, while the same level of ESALs only created around 10 feet of cracks in the thin cells.

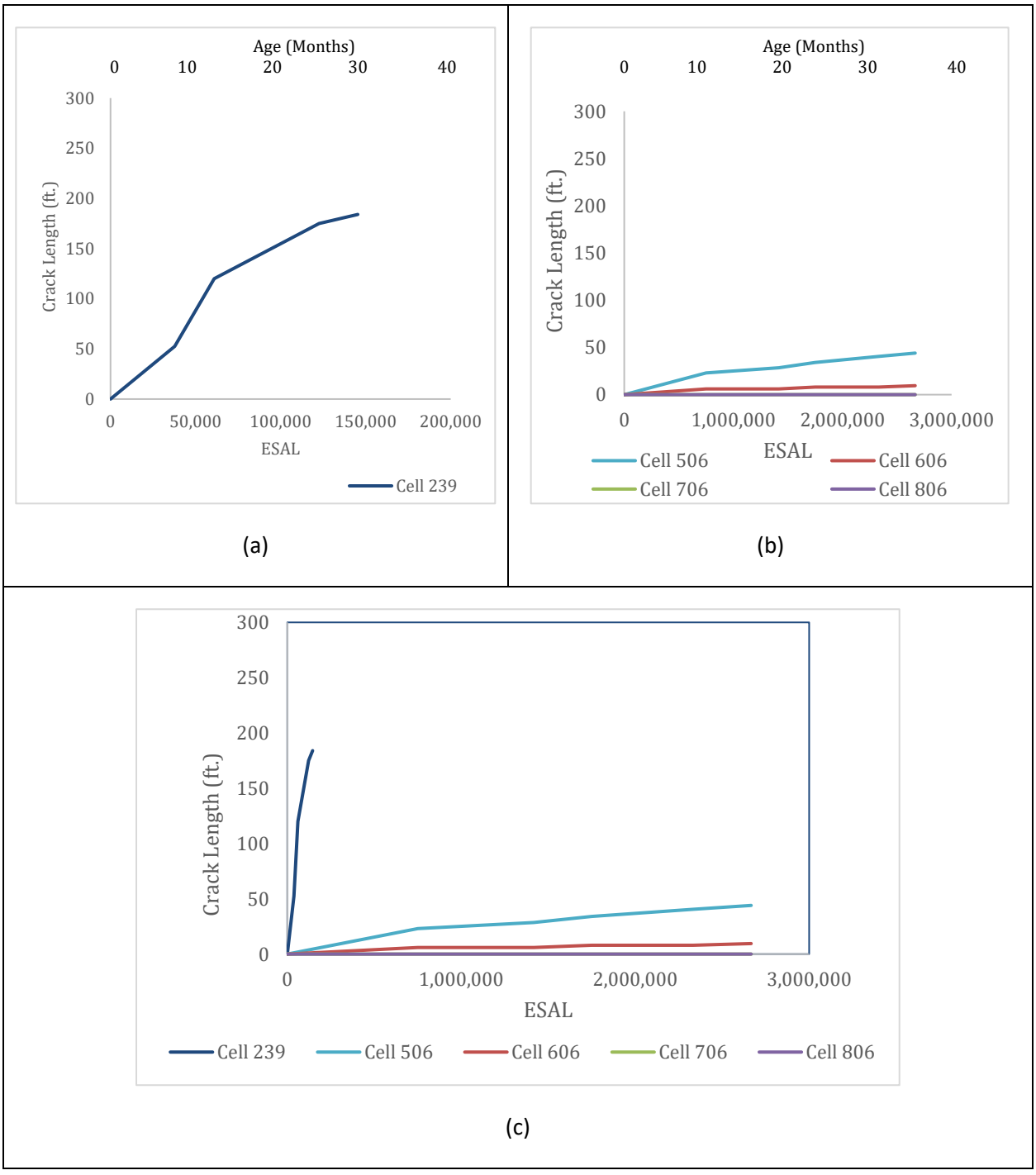

Figure 14: Crack Length vs. ESAL for both **lanes (a) 239 (b) 506,606,706, and 806 (c) 239, 506, 606, 706, and 806.**

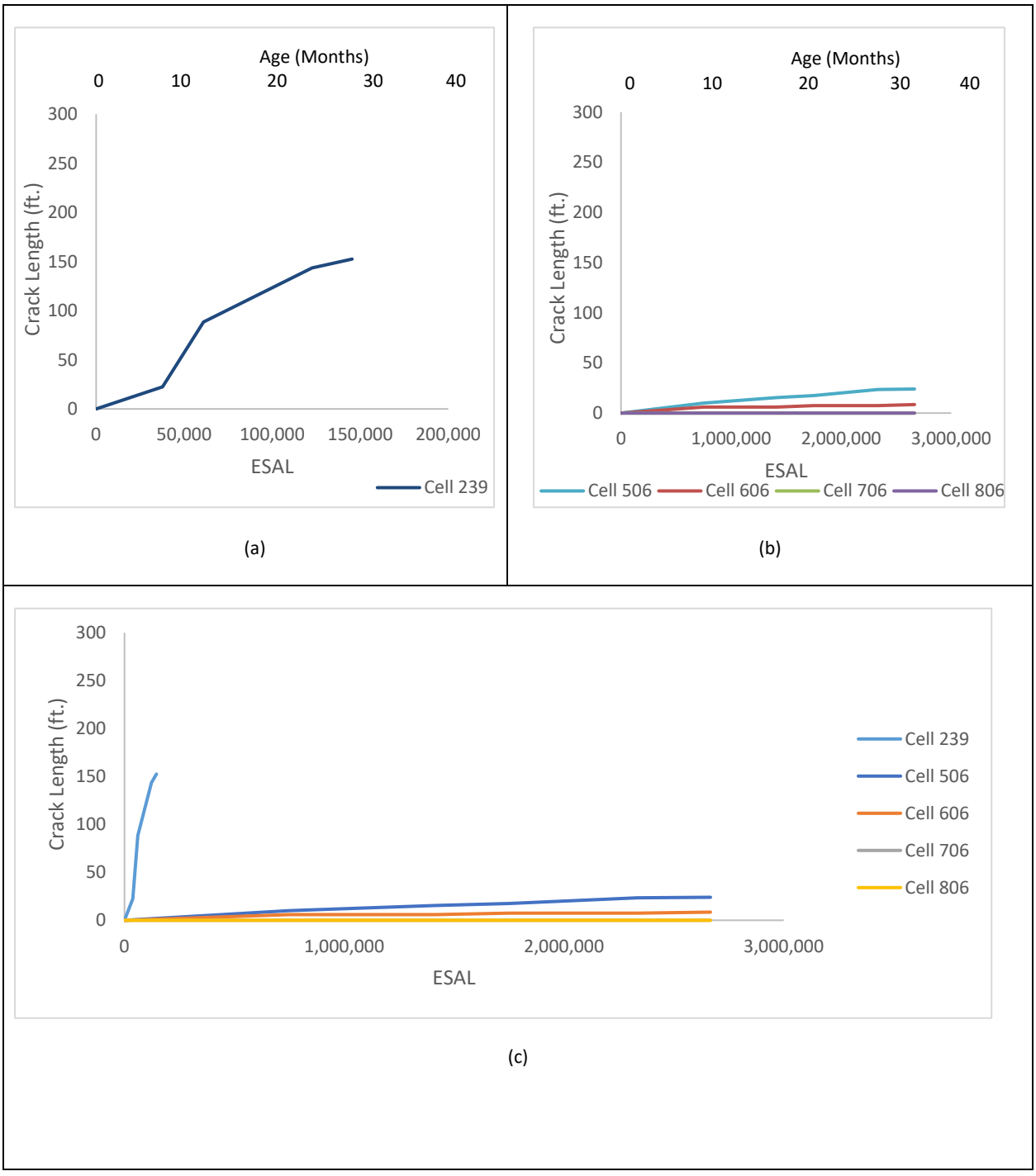

Figure 15: Crack Length vs. ESAL for driving lanes (a) 239 (b) 506,606,706, and 806 (c) 239, 506, 606, 706, and 806.

However, as the numbers of the slabs and the total pavement surface of the cells are different, crack length may also not provide a good comparison between them. A factor termed the 'crack index' has been introduced in this study to include the pavement surface area in the comparison. The crack index

(unit = 1/ft) is the ratio of the crack length in ft and the total area of the cell in ft^2. Figure 16 and Figure 17 compare the crack index between the cells. Based on the crack index, Cell 239 had experienced almost twice the cracks (per unit area) than Cell 506. However, it should be noted that Cell 239 was constructed on a marginal 6 inches thick unstablized base layer, unlike Cells 506-806, which were constructed on a strong 11 inches base layer.

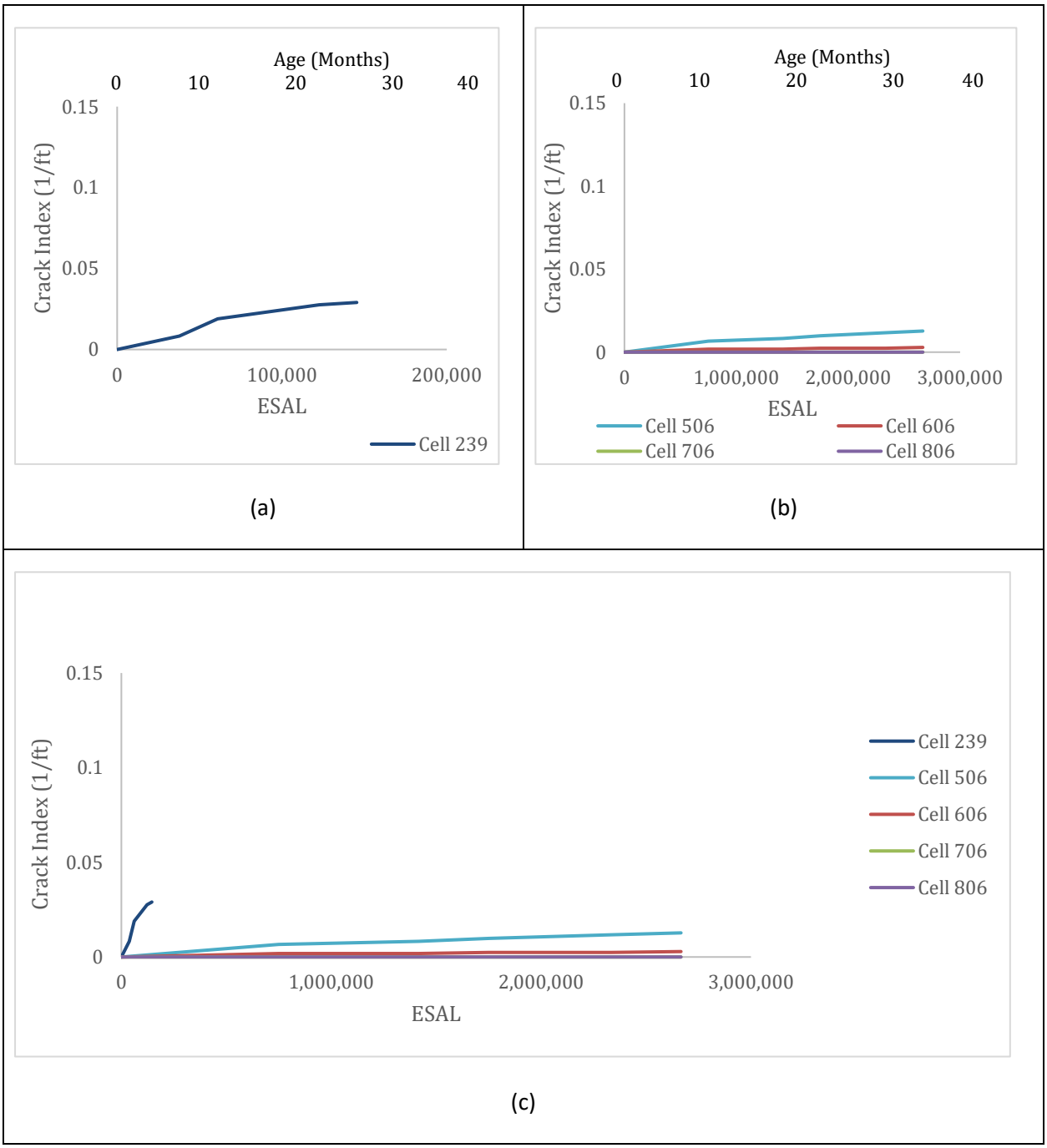

Figure 16: Crack Index vs. ESAL for both lanes (a) 239 (b) 506,606,706, and 806 (c) 239, 506, 606, 706, and 806

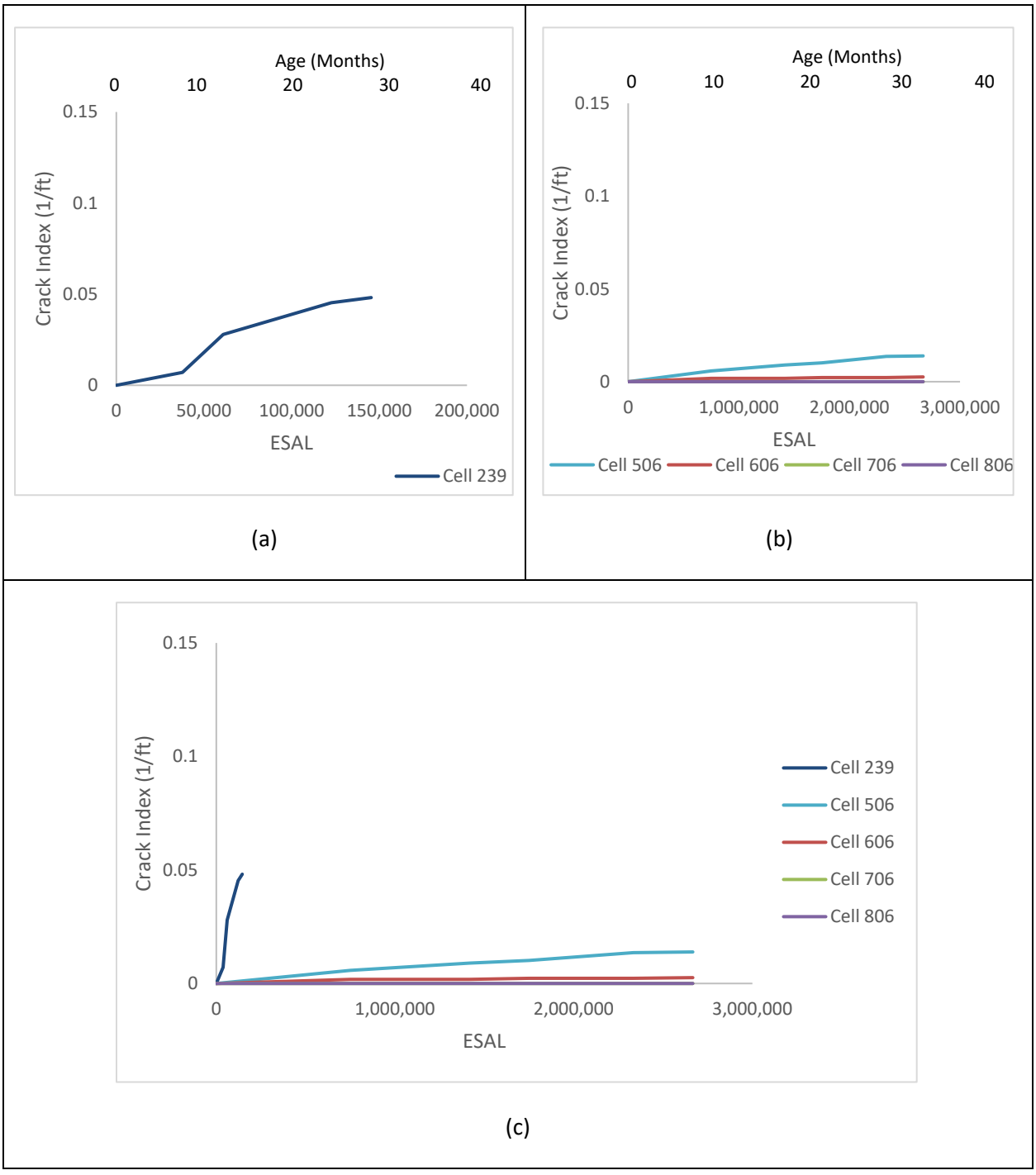

Figure 17: Crack Index vs. ESAL f for driving lanes (a) 239 (b) 506,606,706, and 806 (c) 239, 506, 606, 706, and 806

3.3 Fatigue Cracking Prediction Equations

As observed in the previous sections, Cells 506 through 806 did not experience enough fatigue cracks to derive any conclusions about the influence of fibers on the fatigue cracks. Cells 139 and 239, which experienced significant cracks, have identical fiber dosage and type. Nevertheless, cracking data for Cell 239 was used to study the correlation between the fatigue crack parameters and ESALs for a four-inch-thick FRC pavement on a marginal gravel base. Separate sets of predictive equations were developed for (i) two lanes together and (ii) only the driving lane. The predictive equations for the fatigue crack parameters are provided in Table 6, including the standard error for each equation. Figure 18 shows the comparison between the fatigue crack parameters calculated from the field data and the same predicted by the predictive equations. Figure 19 shows the predictability of the equations, where the measured and predicted values are compared. It may be stated that these equations are only applicable for the 4 inches thick FRC pavements with comparable base thickness, material type, and subgrade properties. The base and subgrade layers' effect could not be included in this study because of the lack of data.

Table 6: Predictive Equations for Fatigue cracking in Cell 239 (4-inch thick FRC pavement)

Fatigue crack parameters	Predictive equations	Standard Error (S)	Traffic
Crack percentage (CP)	$CP = 0.0231303\ ESAL_{total}^{0.569941}$	2.24	$ESAL_{total}$ = Total ESALs in driving and passing lanes
Total crack length (CL)	$CL = 0.030972\ ESAL_{total}^{0.734535}$	19.9	
Crack index (CI)	$CI = 4.88826e\text{-}06\ ESAL_{total}^{0.734535}$	0.00314	
Crack percentage (CP)	$CP = 0.00211199\ ESAL_{DL}^{0.825229}$	4.94	$ESAL_{DL}$ = ESALs only in the driving lane
Total crack length (CL)	$CL = 0.00227361\ ESAL_{DL}^{0.957248}$	21.55	
Crack index (CI)	$CI = 7.17679e\text{-}07\ ESAL_{DL}^{0.957248}$	0.0068	

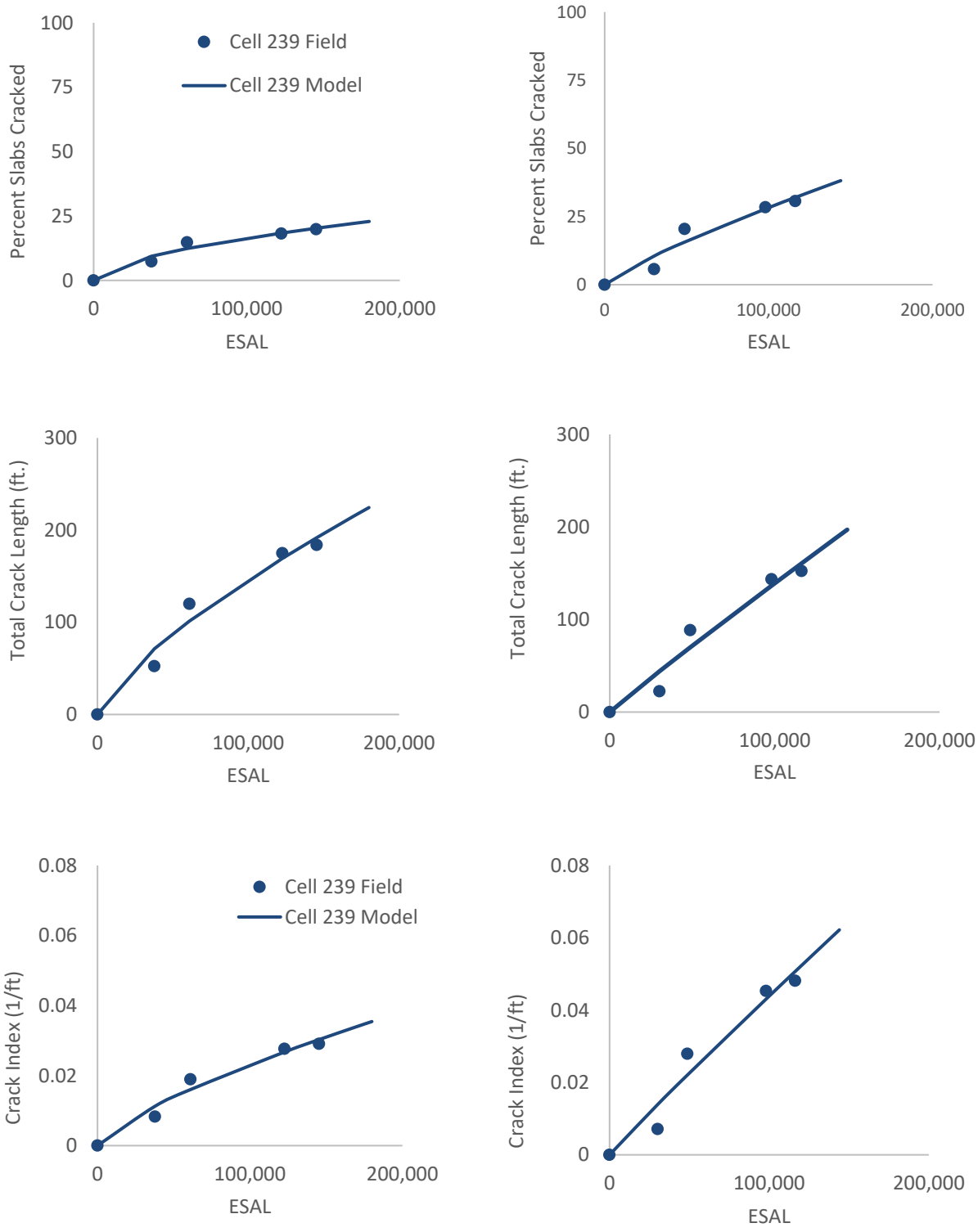

Figure 18: Correlation between the fatigue crack parameters and ESAL for Cell 239 (ultra-thin pavement). Plots on the left are for both lanes, and the right-side plots are for the only driving lane.

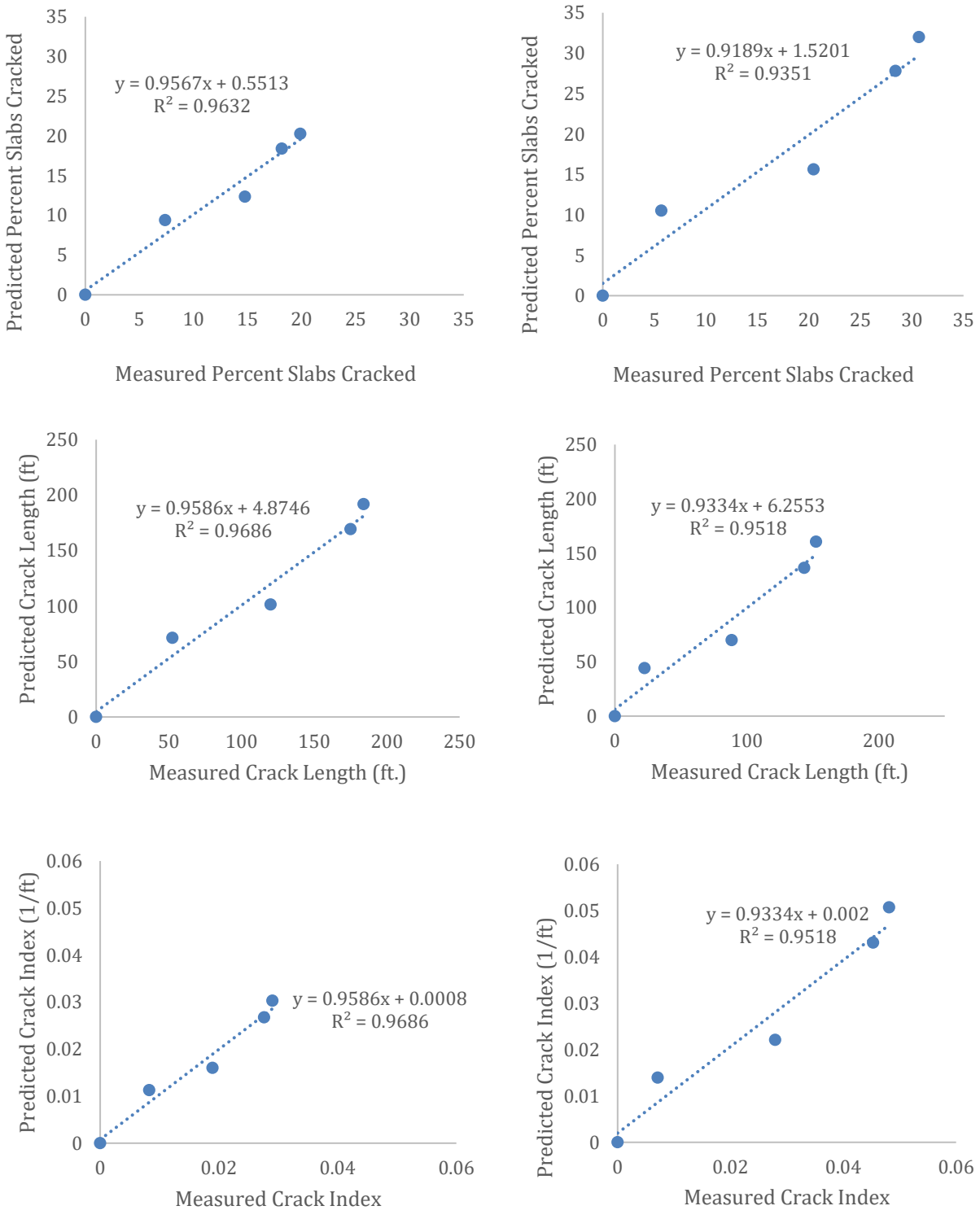

Figure 19: Predictability of the equations developed for Cell 239 (ultra-thin pavement). Plots on the left are for both lanes, and the right-side plots are for the only driving lane.

3.4 FEM Analysis to Determine the Influence of Fibers on Fatigue Life

A small-scale finite element analysis (using ANSYS™) was performed to understand the influence of the fibers on fatigue life. Structural fibers are expected to increase the joint load transfer efficiency (LTE) and joint stiffness, which may reduce the stress and stress-ratio (the ratio of stress in the slab and the modulus of rupture) in the slabs and increase the fatigue life.

In order to quantify the increase in LTE because of fibers, the FWD data collected in this project (provided in Task 4 report) was revisited, and the LTEs measured at three different ESALs levels (at 1, 1.75, and 1.83 million ESALs) were compared between the four cells, Cell 506 through 806, that have various fiber dosages (Figure 20). The above-mentioned three different ESALs were selected because of the availability of the FWD test data at those ESALs. The LTEs measured at 1, and 1.75 million ESALs gave somewhat good correlations between the LTEs and ESALs. The LTEs measured at 1.83 million ESAL did not yield a good correlation as the joints have supposedly deteriorated and fibers' effect had likely minimized. While a very accurate quantification of the LTE gain from a dosage of fiber is not possible from this study., Also, Cell 606 was 6 inches thick, as opposed to 5 inches for the other three cells. If all the cells were 5 inches thick, then the conclusion on the fibers' LTE conclusion could be different. Nevertheless, the laboratory study conducted by Barman et al. (2018) and other similar studies provided enough evidence on the fibers' contribution to the LTE. Based on the above-mentioned facts, it may be conservatively stated that every 2 to 2.5 lb/cy fiber dosage (specific to the fibers used in this particular study) may increase the LTE by 10% approximately. At the same time, it is cushioned that this contribution may change based on the fiber type and pavement design.

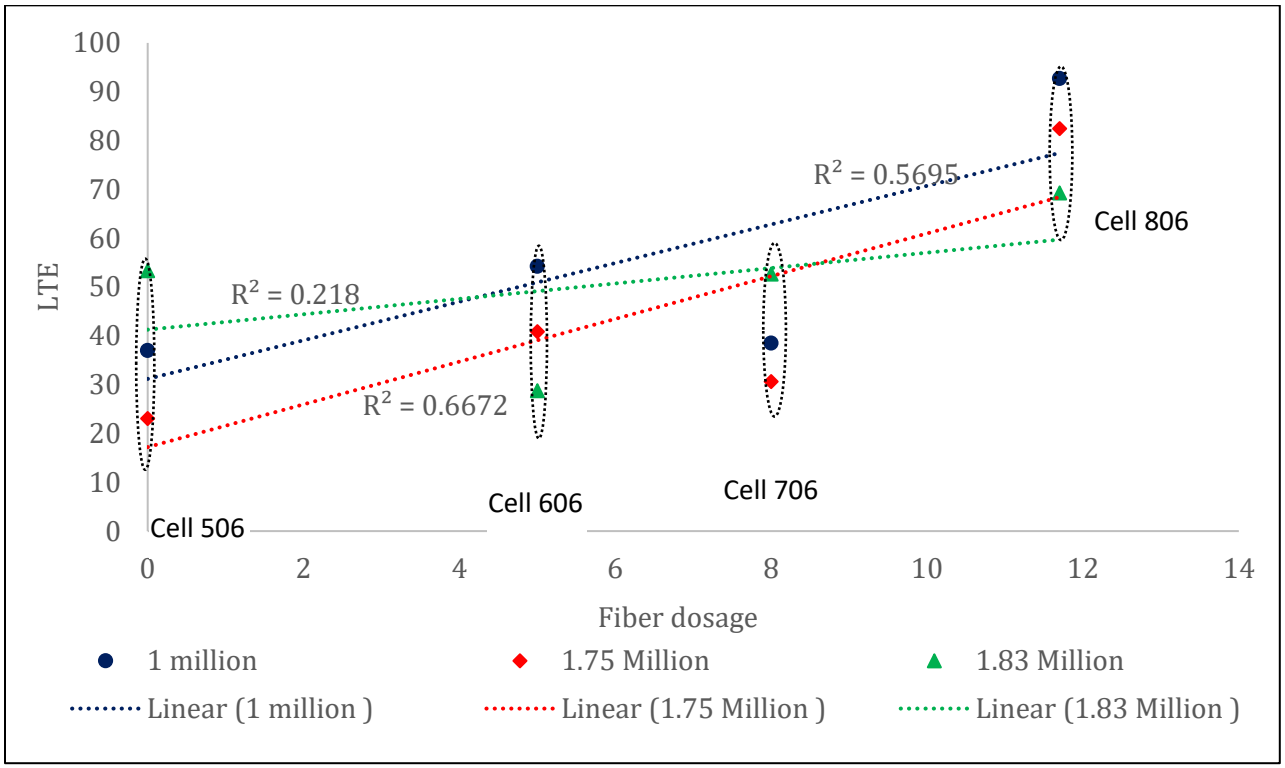

Figure 20: Influence of fiber dosage on the LTE.

Cells 506 through 806 were constructed with strain measuring sensors (static and dynamic). Those sensors were installed at the mid-slab, both near the top and bottom surfaces of the slab (0.5-inch inside the slab), which is not necessarily the most critical location for the fatigue crack initiation in ultra-thin and thin concrete pavements on the unstabilized base layer. To determine stress and strains at other critical locations, FEM models were developed for all four cells. Figure 21 shows a screenshot of the model. Six concrete slabs were considered in the model. The dimensions of the slabs, other layers, and shoulder were the same as was in the field. Properties of concrete and other layers were also matched with the field conditions to the extent possible. The transverse and longitudinal joints were modeled using three-dimensional springs (Matrix 27 element), with spring constants representing the joint shear stiffness (function of LTE, modulus of subgrade condition, the radius of relative stiffness, etc.) and fiber tensile stiffness (resistance offered by fibers against crack width opening) at joints. The spring constants for fibers were derived using the load vs crack width relationships determined in previous laboratory studies conducted at UMD by Barman and Hansen (2018) and Crick (2019).

Wheel load was applied on the outer wheel path near the transverse joint, as shown in Figure 21. The loading area and the stress were assumed to match with that of the MnROAD truck, which is used for applying load repetitions on the low volume test track. Recall that even though these cells were located on the MnROAD mainline and received live interstate traffic, dynamic sensor data was collected using only the MnROAD truck.

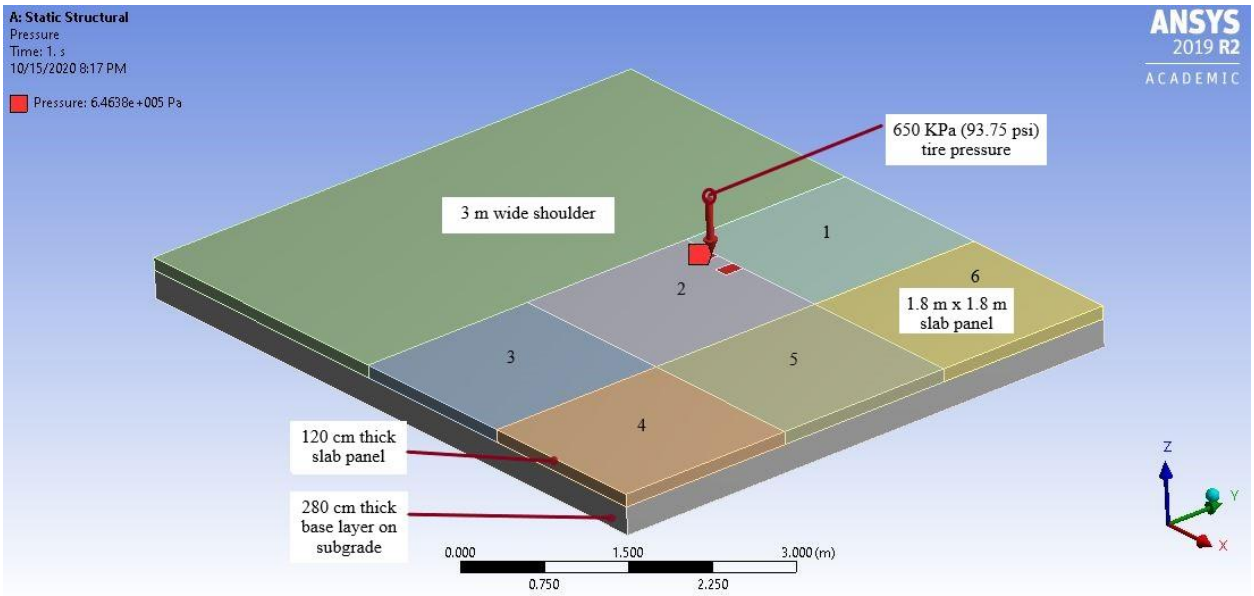

Figure 21: Screenshot of the FEM model.

To estimate the stress values from the strains measured by the strain sensors in the field, correlations were developed between the FEM computed strains and stresses (major principle) for each cell. As the concrete was considered as an elastic material, the obtained relationships were found linear as anticipated. Also, to determine the relationship between the field measured stress (computed from strains) and FEM computed stress values, the same were compared for the mid-slab locations, where field strain data were available (sensor location). The conversion factors were then generated for each cell, which are 0.96, 0.80, 1.06, and 0.56 for the Cells 506, 606, 706, and 806, respectively. These conversion factors were used to convert the FEM calculated stresses to the corresponding field stresses.

Figure 22 shows the stress ratios computed at the critical locations for various LTEs for Cells 506 through 806. The reason for the lower stress ratios for the FRC cells compared to the plain concrete cell (Cell 506) are the (i) slightly higher modulus of rupture for the FRC cells and (ii) fiber stiffness, which acts against the crack width opening below the saw-cut. Figure 22 shows that at a given LTE, the stress ratio is less in the FRC cells. In addition, the LTE is also generally higher for the FRC cells for a given crack width when fibers are in the stretched condition. It may be stated the relationship between the stress ratio and the LTE presented in Figure 22 may change according to the field conditions; nevertheless, the analysis shows the potential to account for the fibers' contribution in calculating the design stress.

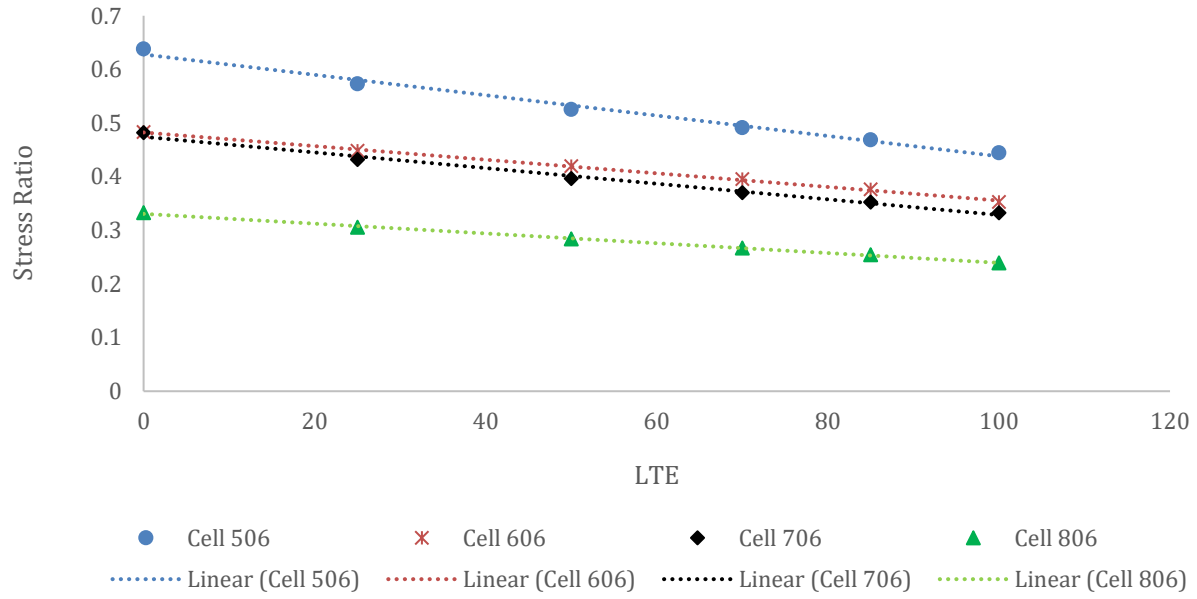

Figure 22: Stress ratio as a function of LTE for Cells 506 through 806.

The reduced stress ratio in the concrete slabs is likely to increase the fatigue life. Based on the limited literature survey conducted, it can be stated that there is no widely accepted fatigue model for ultra-thin and thin FRC pavements, where pavement is directly constructed on the unstabilized base, and the fatigue crack propagation was considered to be affected by the fiber. The MEPDG fatigue model (ARA, 2004) provided below in Equation 1 was used to compute the fatigue lives for various stress ratios that depend on the concrete properties, crack width, and LTE (function of fiber dosages). While an accurate quantification may not be possible with this limited analysis, Figure 23 shows the estimated fatigue lives for the four cells that were constructed with various fiber dosages. While an accurate quantification of fatigue life may not be possible with this limited analysis, Figure 23 shows that higher fatigue life can be achieved if the joints have higher LTE, which can be obtained by using synthetic fibers. However, it shall be noted that the predicted fatigue life values presented in Figure 23 do not represent the real-world values, as LTE keeps changing with time and depend on many other variables. The other important fact is that Equation 1 is for plain concrete and does not depend on the post-crack properties of concrete. The FRCs' essential contribution is in their post-crack performance, so a more accurate prediction of the fatigue life of an FRC pavement or overlay shall be determined using a fatigue model that accounts for the post-crack performance of concrete. Nevertheless, this analysis assures that if LTE can be increased by using synthetic fibers, so is the fatigue life.

.

$$\log\left(N_{i,j,k,l,m,n}\right) = C_1 \cdot \left(\frac{MR_i}{\sigma_{i,j,k,l,m,n}}\right)^{C_2} + \quad 0.4371$$

where,

$N_{i,j,k, \ldots}$ = allowable number of load applications at condition *i, j, k, l, m, n*
MR_i = PCC modulus of rupture at age *i*, psi
$\sigma_{i,j,k, \ldots}$ = applied stress at condition *i, j, k, l, m, n*
C_1 = calibration constant = 2.0
C_2 = calibration constant = 1.22

(Equation 1)

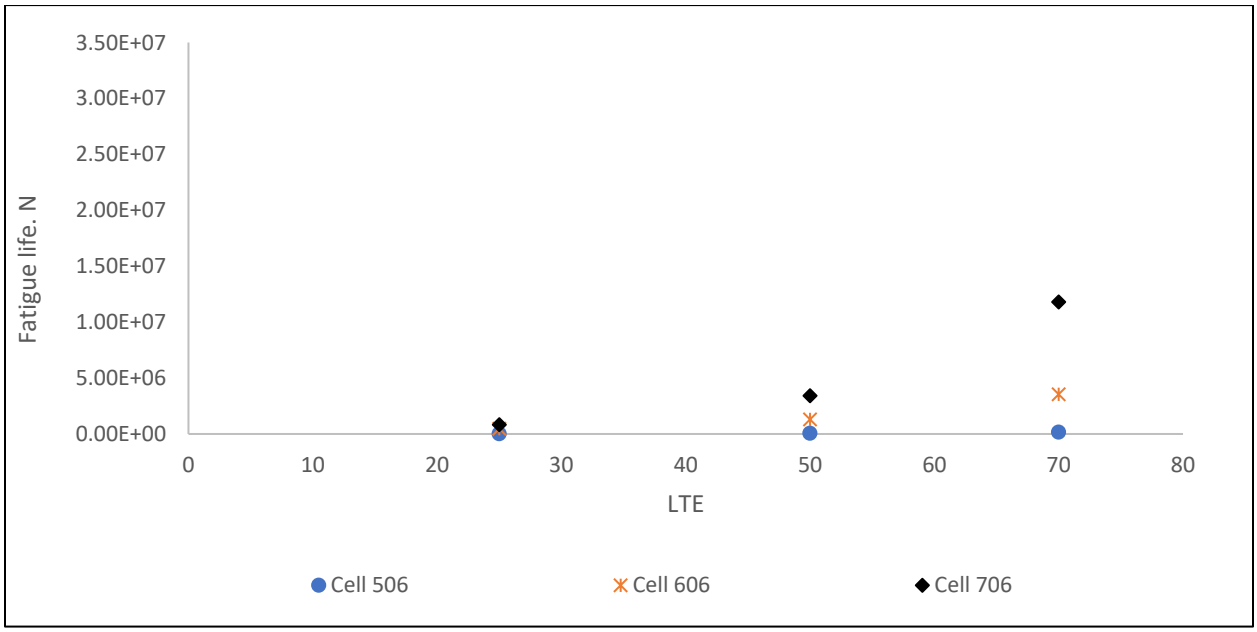

Figure 23: Demonstration of the benefit of fibers in Fatigue life (Cell 506- no fiber; Cell 606- 5lb/cy, Cell 706 – 8 lb/cy fiber)

CHAPTER 4: TASK 5 FINDING ON THE EFFECT OF FIBERS ON SLAB SIZE

4.1 Fatigue crack data

Cells 705 and 805 were constructed to study whether the inclusion of fibers can influence the slab size, more specifically, if fibers can help increase the slab size to reduce the construction cost. Cell 705 was constructed in 2017 as a 5-inch thick unbonded concrete overlay placed over a nonwoven geotextile fabric, secured to an existing 7.5-inch-thick concrete pavement originally constructed in 1993. Cell 705 was constructed with “large” slabs for the given thickness, 12 ft x 12 ft (passing lane), and 14 ft W x12 ft L (driving lane). Figure 24 shows photographs of typical longitudinal, transverse, and corner cracks that developed in Cell 705 during the first year of service. These kinds of cracks propagated with age and ESALs, as shown in Figure 26, and the driving lane of the cell was eventually taken out of service during the third year of service, after approximately 3 million ESALs.

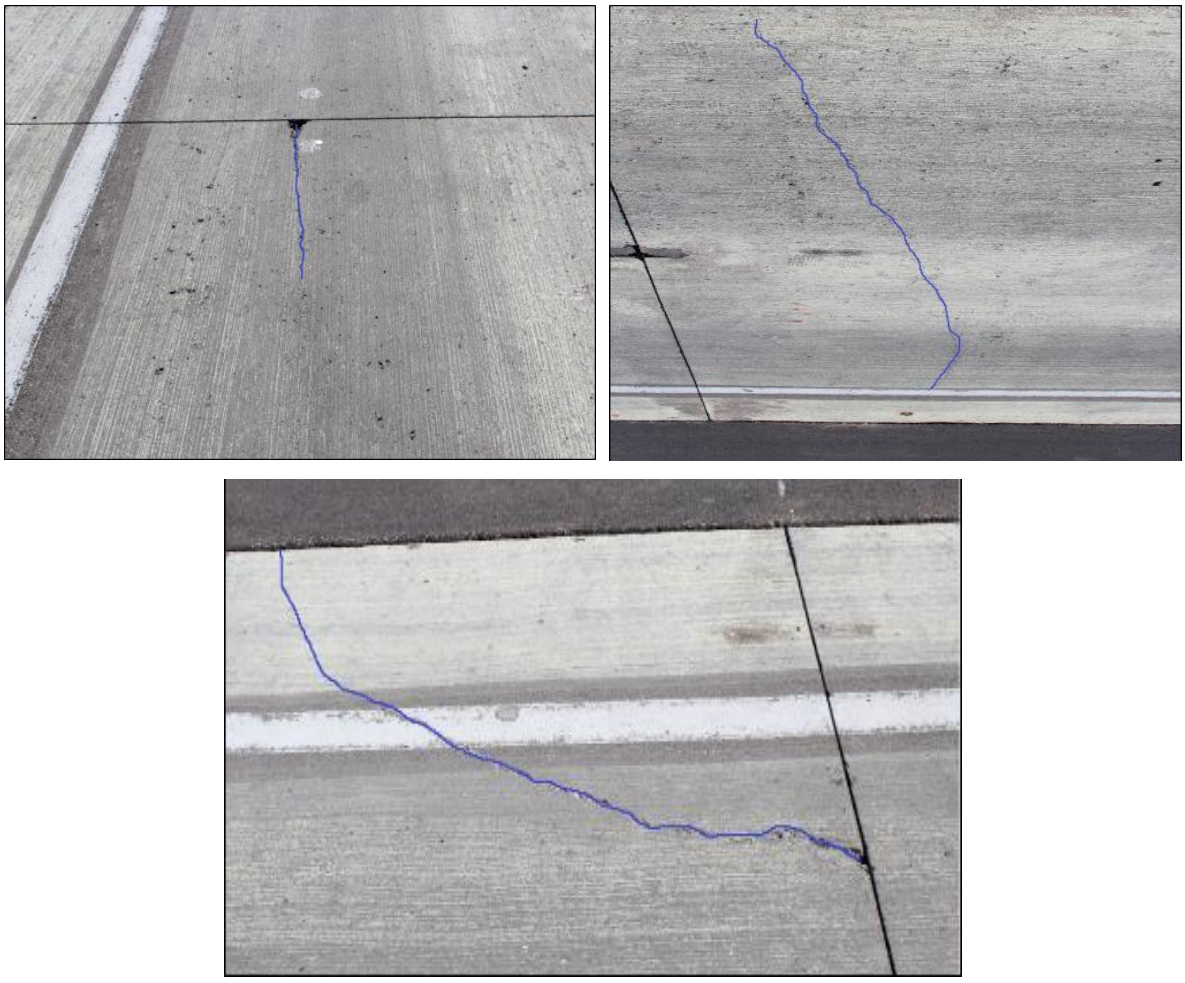

Figure 24: Typical cracks that developed in Cell 705 during the first year of service (highlighted for clarity).

Figure 25: Cracks in Cell 705 in the third year of service.

Cell 805, which was also constructed as a 5-inch thick unbonded concrete overlay, had narrower slabs (6 to 8 ft wide x 12 ft long) compared to Cell 705, as shown in Table 1. This cell also experienced longitudinal cracks, transverse cracks, and corner cracks. Figure 26 shows photographs of typical cracks in Cell 805 observed in the first year of service. Similar to Cell 705, this cell also deteriorated and was finally taken out of service during the third year of service, after approximately 3 million ESALs. Figure 27 shows cracked slabs in Cell 805 in the third year of service.

Color-coded distress maps for Cell 705 and 805 are provided in Figure 28. Figure 29 presents the cumulative numbers of cracks on different dates for the two cells. Based on the distress survey data available until March 2020, 11 out of 22 panels were cracked in Cell 705, of which eight were in the driving lane; a total of 50% slabs have cracked after 2.7 million ESALs. For Cell 805, 14 out of 40 slab panels have cracked, of which 13 were in the driving lane; 65% of the slabs in the driving lane and 35% (15% less than Cell 705) of total slab panels cracked after 2.7 million ESALs. Cell 705 experienced more longitudinal cracks than transverse and corner cracks. The reason for the larger number of longitudinal cracks in this cell may be due to the higher amount of curvature of thin wider slabs, which resulted in

higher amount of stresses in combination of the wheel load. Cell 805 experienced longitudinal, transverse, and corner cracks in comparable quantities. Similar to Cell 705, the driving lane of this cell was eventually taken out of service during the third year of service, after approximately 3 million ESALs.

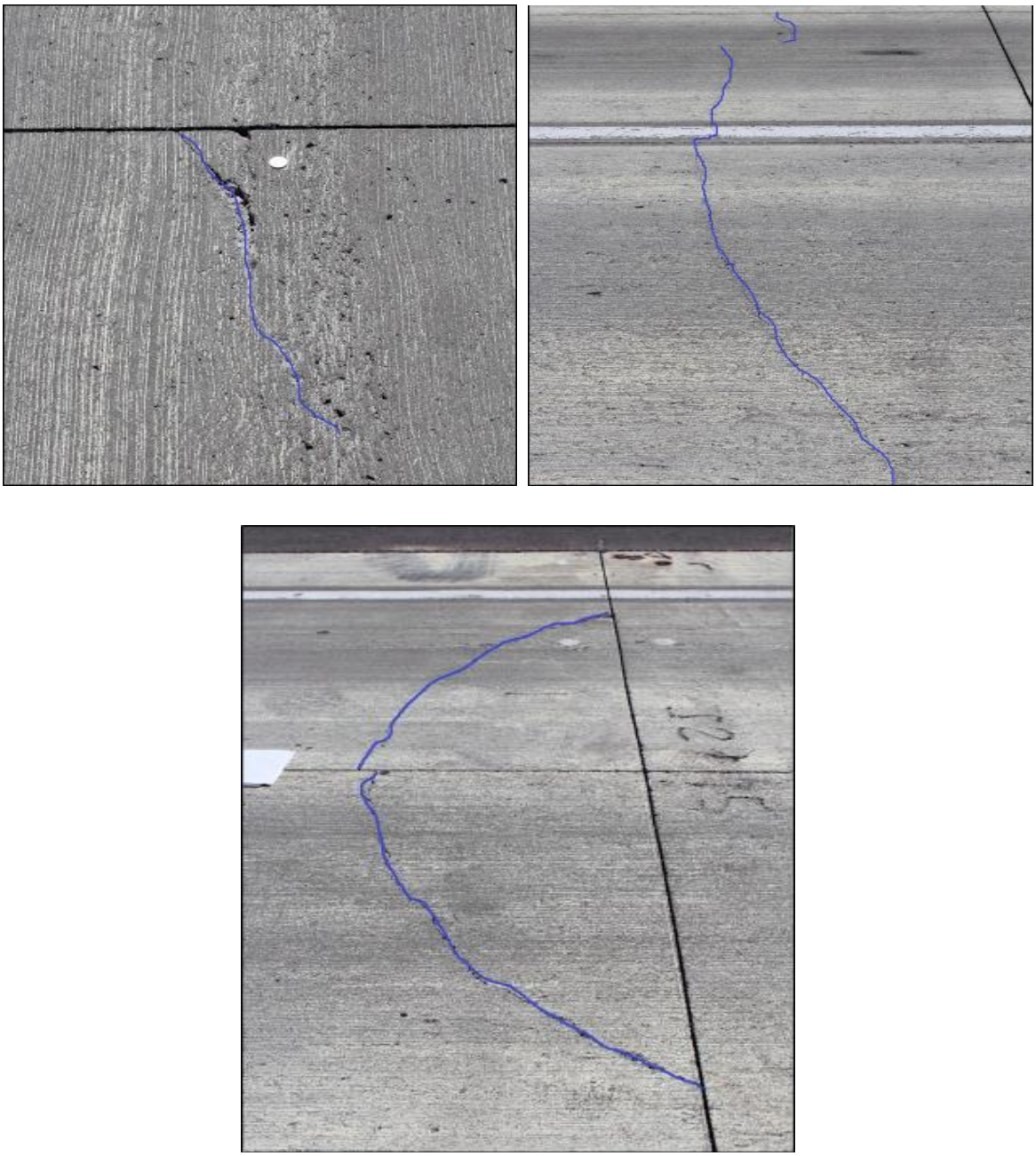

Figure 26: Typical cracks observed in Cell 805 (highlighted for clarity).

Figure 27: Cracks in Cell 805 in the third year of service.

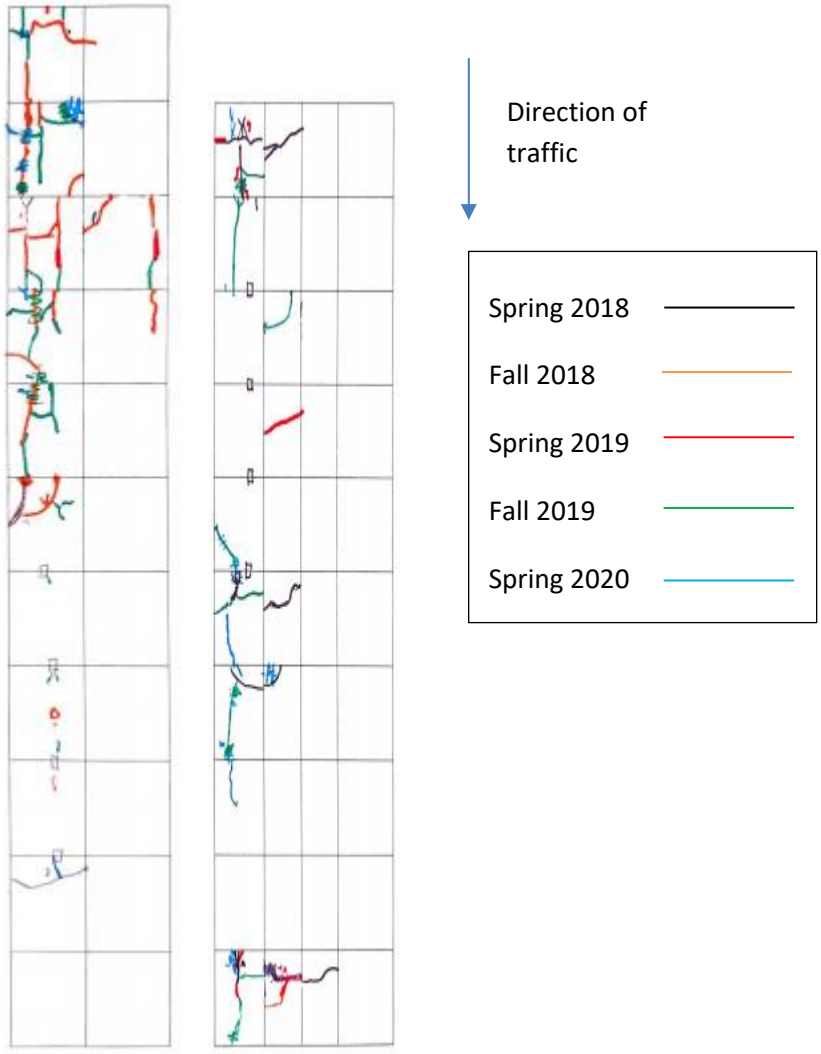

Figure 28: Distress Survey Maps (a) Cell 705 (b) Cell 805.

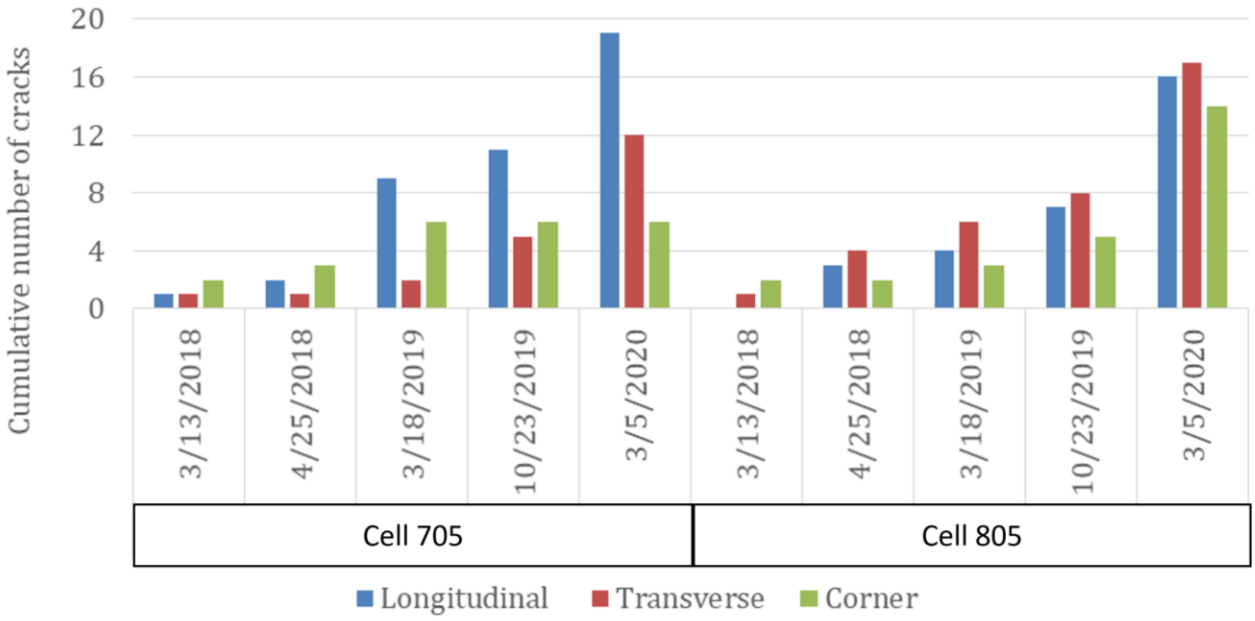

Figure 29: Cumulative number of various cracks in Cell 705 and 805.

4.2 Fatigue Crack Progression with Age and Traffic

As mentioned above, it was seen that Cell 805 with smaller slabs resulted in less percentage of cracked slabs (35%) than Cell 705 (50%) after three years of traffic and climate. Figure 30 through Figure 32 compare fatigue crack parameters between Cells 705 and 805. When the comparison was made with respect to the crack length, it was found that the total length of the cracks (both lanes) in Cell 705 was 30% more than Cell 805 after 2. 7 million ESALs, as shown in Figure 30. However, when the comparison was made with respect to crack index (defined in the previous section), the difference between the two cells has minimized, the driving lanes of both the cells experienced almost the same crack index, which indicates the crack length on the unit pavement area is the same for both the cells. Therefore, it may be stated that fibers' influence on the slab size was minimal when crack length on the unit pavement area is considered for the comparison, but otherwise, Cell 705 resulted in a higher percentage of cracked slabs.

The above finding suggests that construction of wider panels with synthetic fibers (at least for the dosages and type used in Cells 705 and 805) may not be a better design than using narrower panels in terms of performance.

The preference for the construction of narrower panels vs wider panels shall not, however, be decided only on the total number of cracks or crack index. Other factors like the rate of crack progression and ease of repair of the cracked slabs shall also be considered. Based on Figure 30 and Figure 31, it appears

that smaller panels (Cell 805) develop cracking at a slower pace, which may be an advantage to delay the repair work. But whether it is easy to repair more numbers of narrower panels than a smaller number of wider panels, is a different question and shall be considered while making the decision for slab size. The faulting and riding quality of these two cells described in the following chapters will provide more insights into the performance comparison.

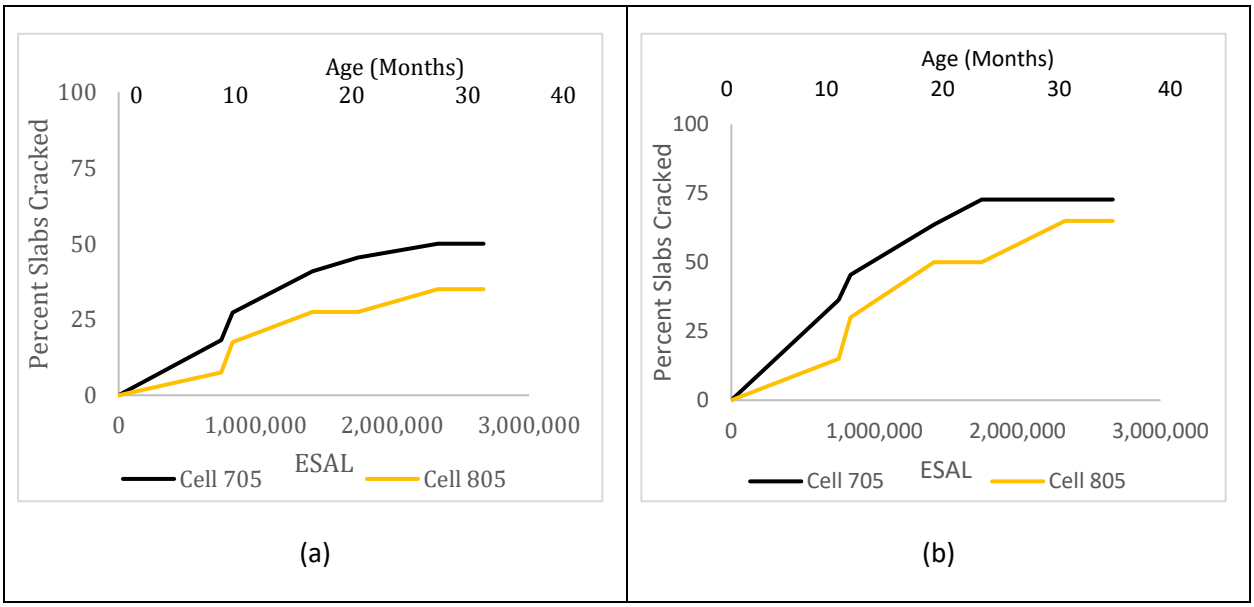

Figure 30: Percent slabs cracked vs ESAL for Cells 705 and 805 (a) Driving and Passing lane combined (b) Driving Lane only.

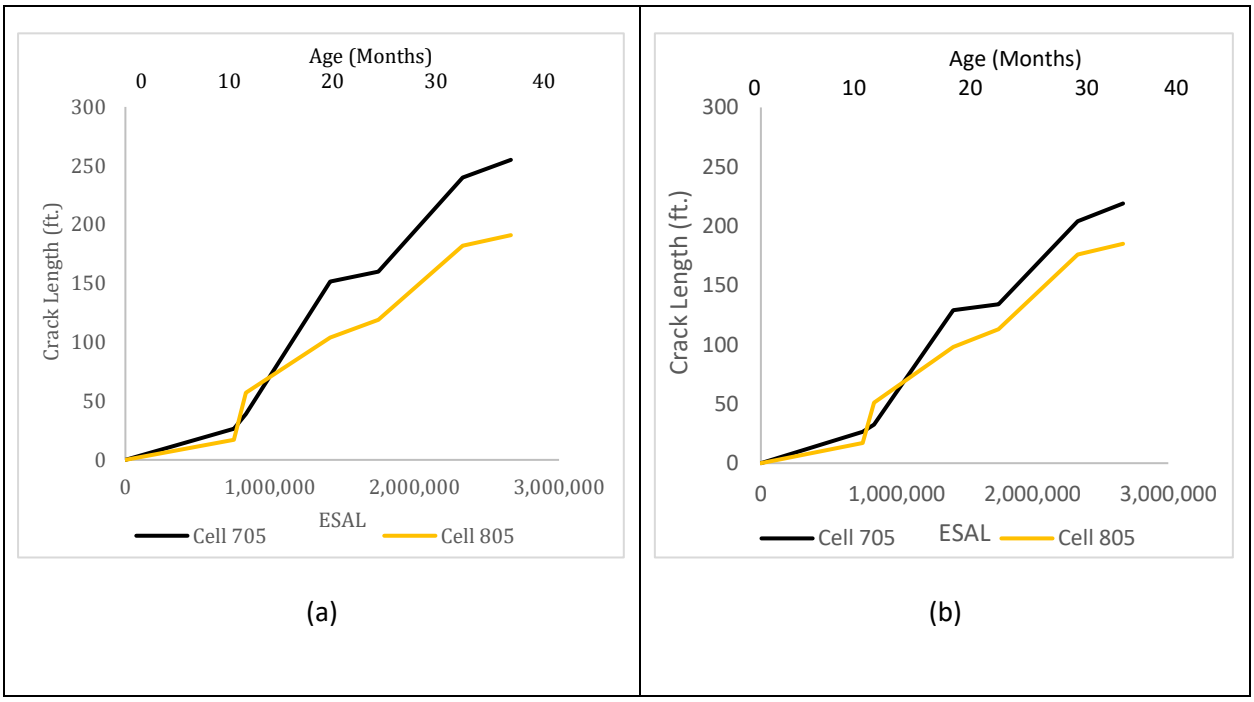

Figure 31: Crack Length vs ESAL for Cells 705 and 805 (a) Driving and Passing lane combined (b) Driving Lane only.

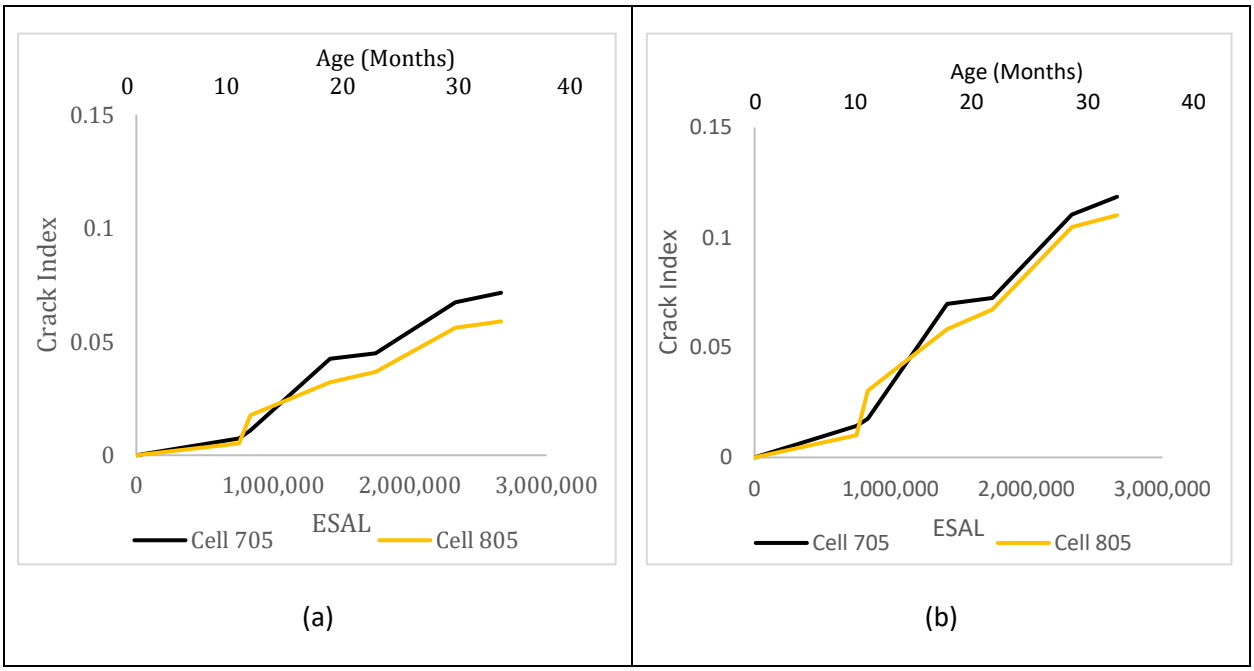

Figure 32: Crack Index vs ESAL for Cells 705 and 805 (a) Driving and Passing lane combined (b) Driving Lane only.

4.3 Fatigue Cracking Prediction Equations

Separate fatigue cracking predictive equations were developed for (i) both lanes together and (ii) for the driving lane alone. Predictive equations are provided in Table 6. Figure 18 shows the comparison of the fatigue crack parameters calculated from the field data and the same predicted by the predictive equations. It may be stated that these equations are only applicable for the 5 inches thick FRC overlays that have field conditions comparable to Cells 705 and 805. The interlayer effect could not be included in this study because of the lack of data. Figure 34 shows the predictability of the equations, where the measured and predicted values are compared.

Table 7: Predictive Equations for Fatigue cracking in for 5 inches thick unbonded concrete overlays.

Fatigue crack parameters	Predictive equations	Standard Error (S)	Traffic
Crack percentage (CP)	$CP = ESAL_{total}^{.60}$ x (0.00238127 +3.5327e-05 x SA	3.99	$ESAL_{total}$ = Total ESALS in driving and passing lanes SA = Slab area (ft^2)
Total crack length (CL)	$CL = ESAL_{total}^{.74}$ x (0.00209012 +1.36573e-05 x SA	32.95	
Crack index (CI)	$CI = ESAL_{total}^{.74}$ x (3.01071e-07 +5.81385e-09 x SA)	0.011	
Crack percentage (CP)	$CP = ESAL_{DL}^{.60}$ x (0.00754828 +3.88817e-05 x SA)	6.8	$ESAL_{DL}$ = ESALS only in driving lane
Total crack length (CL)	$CL = ESAL_{DL}^{.74}$ x (0.00287066 +8.41359e-06 x SA)	29.14	
Crack index (CI)	$CI = ESAL_{DL}^{.74}$ x (9.084e-07 + 9.03187e-09x SA)	0.02	

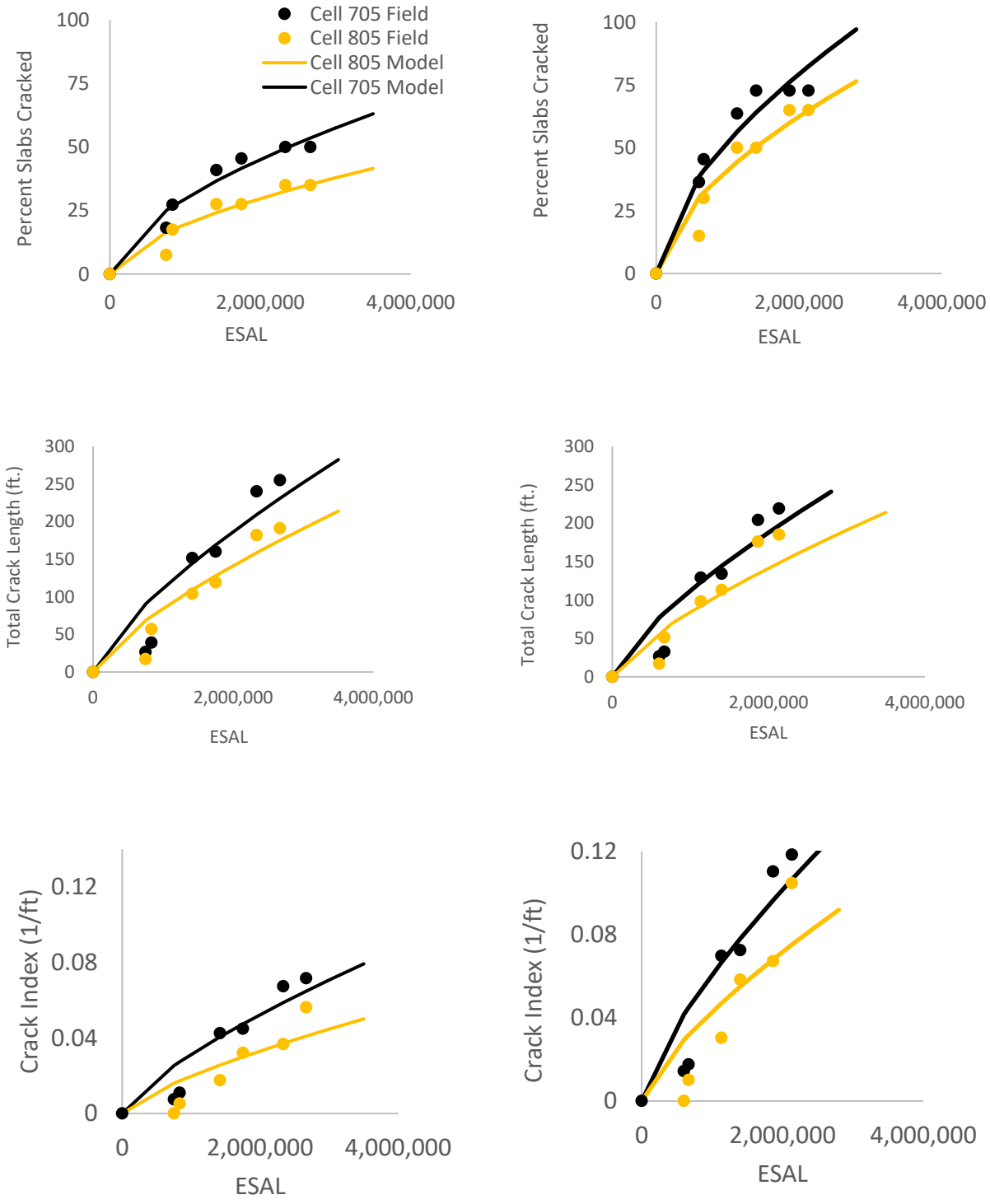

Figure 33: Correlation between the fatigue crack parameters and ESAL for 5 inches thick concrete overlays. Plots on the left are for both lanes, and the right-side plots are for the only driving lane.

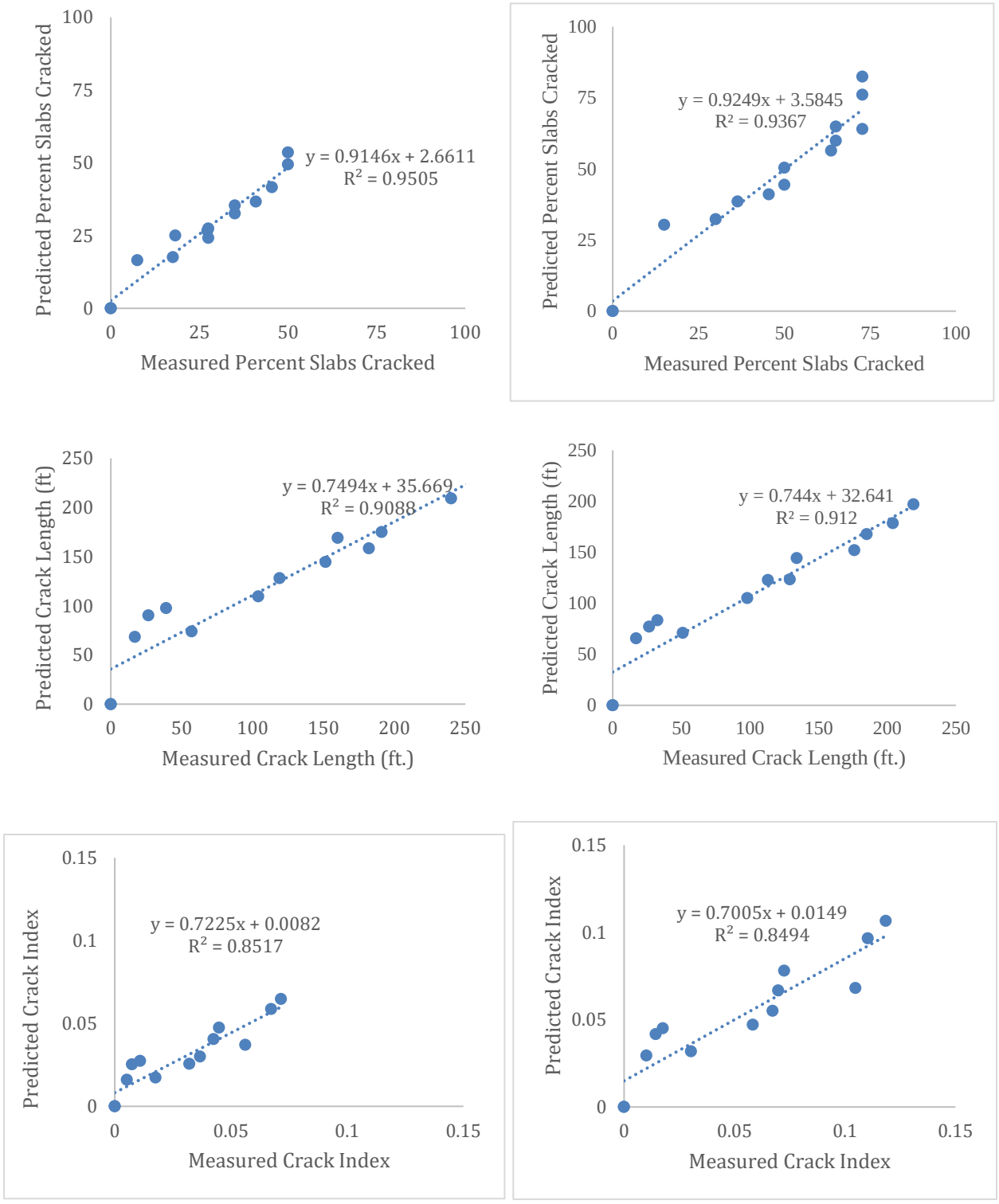

Figure 34: Predictability of the equations developed for unbonded concrete overlays (ultra-thin pavement). Plots on the left are for both lanes, and the right-side plots are for the only driving lane.

CHAPTER 5: CONCLUSION

This report included the findings from Task 3 and Task 5. The major conclusions drawn from these two tasks are summarized below:

- The thickness of Cell 139 was 3 inches, which is extremely thin on a 6-inch unstabilized aggregate base. The cracks observed in this cell were more like bottom-up fatigue cracks of asphalt pavement with shattered slabs along the wheel path.
- The contribution of the fibers (@8lb/cy fiber, 30% RSR) on Cell 139 is not clear. Given the 3-inch thickness of the slab, it can be stated the concrete, or the overall pavement structure was too weak for yielding any fiber benefit. However, it was observed that the fibers were able to hold the cracked slab pieces together, which otherwise might have been pressed into the base, or become scattered rather quickly. Also, it is unclear whether the severity of the distress for Cell 139 would have been this much, had the Cell not have been loaded by construction traffic at a very early age.
- Cell 239 (4-inch thick) has performed much better than Cell 139. The dominant distress for Cell 239 was longitudinal cracking along the wheel path. This behavior coincides with the behavior observed in other thin concrete pavement overlay structures
- With respect to fatigue cracking, Cells 506 through 806 have performed better than all other FRC cells in this study, with only a few cracks in three slabs of Cell 506 (no fiber).
- Although data was limited, preliminary fatigue crack predictive equations were developed for Cell 239. Correlation with field distress data was reasonable.
- As Cells 506 through 806 have not experienced enough cracks yet, it was difficult to quantify the contribution of fibers in mitigating fatigue cracks. These cells have successfully carried more than 3 million ESALs. This observation indicates that the critical distress for the small panel thin concrete pavements on the relatively stiff base layer may not be the fatigue cracking, but the other distresses like faulting (which was observed).
- The study included a finite element analysis. Through this analysis, it was shown that structural fibers have the potential to decrease the stress ratio in the critical locations.
- Wide-paneled (~12 ft wide, Cell 705) thin unbonded overlays experienced a higher percentage of cracked slabs and total crack length than the narrow-paneled ones (~6 ft wide, Cell 805).

However, when total crack length over the unit pavement surface area (known as crack index) was considered, the difference in cracking between the cells was found to be less.

Lastly, it should be cautioned that the results from this experiment represent the behavior of three dosages of one synthetic fiber and one concrete mixture. It should not be construed that the results represent the behavior of other types and dosages of synthetic fibers or concrete mixtures, for that matter.

REFERENCES

[1]. ASTM-C1609. (2010). Standard Test Method for Flexural Performance of Fiber-Reinforced Concrete (Using Beam With Third-Point Loading). American Society for Testing and Materials West Conshohocken, PA.

[2]. ARA, Inc., ERES Division. *Guide for Mechanistic-Empirical Design of New and Rehabilitated Pavement Structure: Appendix KK Transverse Cracking of JPCP.* National Cooperative Highway Research Program, Transportation Research Board, National Research Council, August 2003.

[3]. Crick, C. (2019). Joint Performance Behavior of Fiber Reinforced Concrete, MS Thesis, University of Minnesota Duluth. MN.

[4]. Barman, M., and B. Hansen, (2018). *Comparison of Performances of Structural Fibers and Development of a Specification for Using Structural Fibers in Thin Concrete Overlays,* Final Report, Minnesota Department of Transportation, St. Paul, MN.

[5]. MnDOT (2019). "*MnROAD Semi Tractor Trail*er". Minnesota Department of Transportation, St. Paul, MN. <http://www.dot.state.mn.us/mnroad/data/pdfs/MnROADSemiDescriptions(March%202013).pdf https://www.dot.state.mn.us/mnroad/data/traffic.html>

[6]. Deusen, Dave V., Burnhum, T., Dai S., Geib, J., Hanson, C., Izevbekhai, B., Johnson, E., Palek, L., Siekmeier, J., Vrtis,M., and Worel, B. *Report on 2017 MnROAD Construction Activities.* Report Number: MN/RC 2018-16. Minnesota Department of Transportation, May 2018.

APPENDIX

Table A1: ASTM C1609 test results

Specimen ID	MOR (psi)	Residual Strength Ratio (%)	Residual Strength (psi)
Cell 506-7day #1	465	-	-
Cell 506-7day #2		-	-
Cell 506-28day #1	650	-	-
Cell 606-7day #1	465	26.4	122.7
Cell 606-7day #2			
Cell 606-28day #1	635	19.4	124.1
Cell 606-28day #2			
Cell 706-7day #1	480	29.3	140.6
Cell 706-7day #2			
Cell 706-28day #1	675	23	156.4
Cell 706-28day #2			
Cell 806-7day #1	525	45.2	237.3
Cell 806-7day #2			
Cell 806-28day #1	680	37.4	254.3
Cell 806-28day #2			
Cell 139/239-28day #1	610	30.4	185.4
Cell 139/239-28day #2			
Cell 139/239-28day #3			
Cell 705/805-28day #1	542	21.5	116.5
Cell 705/805-28day #2			
Cell 705/805-28day #3			
Cell 705/805-28day #4			

Table A2: Properties of Concrete used in the NRRA cells

Fresh Concrete Properties								
Cell No.	139	239	705	805	506	606	706	806
Box Test	1,1,1,1	1,1,1,1	2,1,1,2	2,1,1,2	2,2,1,2	2,1,2,2	1,2,2,2	2,1,1,2
SAM No.	0.27	0.3	0.33	0.3	0.3	0.3	0.23	0.31
ASTM C231, Fresh air (%)	8.1	8.0	6.0	7.5	5.4	7.7	7.2	6.6
Hardened Concrete Properties								
Cell No.	139	239	705	805	506	606	706	806
Compressive strength, psi	1,910 (3 days)		2,990 (3 days)		2,740	2,360	2,690	2,510
	2,630 (7 days)		3,720 (7 days)		3,360	3,020	3,050	3,170
	3,800 (28 days)		- (28 days)		4,520	4,050	4,140	4,120
Surface resistivity 28 days, KW-cm	21.3		-		24.3	22.2	23.4	24.4
Air Content, %	8.3		-		5.8	8.5	6.3	6.5
Spacing factor, in.	0.0015		-		0.002	0.002	0.002	0.002

Specific surface, in2/in3	1,485	-	1,600	1,540	1,990	1,630
Dynamic Modulus of elasticity, 28 days	-	-	6.22 x 10^6 psi	5.21 x 10^6 psi	5.56 x 10^6 psi	4.97 x 10^6 psi
Poisson's Ratio	-	-	0.20	0.20	0.18	0.21
Static Modulus of Elasticity, 28 days	-	-	5.4 x 10^6 psi	4.3 x 10^6 psi	4.72 x 10^6 psi	4.61 x 10^6 psi